

Small-volume effect enables the spine robust, sensitive and efficient information transfer

Masashi Fujii,¹ Kaoru Ohashi,¹ Yasuaki Karasawa,² Minori Hikichi,¹ and Shinya Kuroda^{1,3,*}

¹*Department of Biological Sciences, Graduate School of Sciences, University of Tokyo, Hongo 7-3-1, Bunkyo-ku, Tokyo, 113-0033, Japan*

²*Department of Neurosurgery, Graduate School of Medicine, University of Tokyo, Hongo 7-3-1, Bunkyo-ku, Tokyo 113-0033, Japan*

³*CREST, Japan Science and Technology Agency, Hongo 7-3-1, Bunkyo-ku, Tokyo 113-0033, Japan*

*Corresponding author: skuroda@bs.s.u-tokyo.ac.jp

Abstract

Why is the spine of a neuron so small that only small numbers of molecules can exist and reactions inevitably become stochastic? Despite such noisy conditions, we previously showed that the spine exhibits robust, sensitive and efficient features of information transfer using probability of Ca^{2+} increase; however, their mechanisms remains unknown. Here we show that the small-volume effect enables robust, sensitive and efficient information transfer in the spine volume, but not in the cell volume. In the spine volume, intrinsic noise in reactions becomes larger than extrinsic noise of input, making robust information transfer against input fluctuation. Stochastic facilitation of Ca^{2+} increase occurs in the spine volume, making higher sensitivity to lower intensity of input. Volume-dependency of information transfer enables efficient information transfer per input in the spine volume. Thus, we propose that the small-volume effect is the functional reasons why the spine has to be so small.

The spine is a platform of a neuron where input timing information from other neurons is integrated, and is extremely small^{1,2}. For example, in a parallel fiber (PF)-cerebellar Purkinje cell synapse, the volume of spine is approximately $0.1 \mu\text{m}^3$ where the number of molecules are limited to tens to hundreds (Fig. 1a, see also Fig. 7), and is 10^4 -fold smaller than the cell body ($5,000 \mu\text{m}^3$) (Fig. 1a, see also Fig 7)³⁻⁵. Under such conditions, reactions in the spine inevitably become stochastic and inputs are fluctuated due to low numbers of molecules in the small volume⁶⁻¹⁰. Intuitively, such noisy conditions are disadvantageous for information processing. Why is the spine so small? This is one of the fundamental questions in neuroscience and biological information processing.

Cerebellar Purkinje cells receive two inputs. One is PF inputs from granular neurons that are thought to code sensorimotor signals, and the other is a climbing fiber (CF) input from inferior olivary nucleus that is thought to code error signal¹¹⁻¹³. Conjunctive PF and CF inputs but not either PF or CF inputs alone has been shown to induce large Ca^{2+} increases by positive feedback loop via IP_3 (inositol trisphosphate)-induced Ca^{2+} release (IICR)^{14,15}, leading to long-term decreases of synaptic strength that are known as cerebellar long-term depression (LTD)¹⁶, a tentative molecular basis of cerebellar motor learning^{17,18}. It has experimentally been shown that large Ca^{2+} increase occur when PF and CF inputs are coincident at a given synapse within a 200 msec time window, and that Ca^{2+} increase against the timing between PF and CF inputs shows a bell-shaped response (Fig. 1c)¹⁵. We have previously developed detailed biochemical deterministic model of Ca^{2+} increase in a PF-cerebellar Purkinje cell synapse, and reproduced the PF- and CF-timing dependent Ca^{2+} increase¹⁹. In addition, by reducing this model, we have also made the simple deterministic model and extracted essential framework of the network for PF and CF inputs dependent Ca^{2+} increase^{20,21}.

However, in the spine, the number of molecules is limited to tens to hundreds; thus, reactions should behave stochastically rather than deterministically. Indeed, it has experimentally been shown that, the coincident PF and CF inputs stochastically induce Ca^{2+} increases; in some cases, large Ca^{2+} increases are observed, whereas in other cases, they are not (Fig. 1b, c). In addition to the intrinsic noise due to the stochastic fluctuation of Ca^{2+} increase, PF inputs has been shown to fluctuate⁸⁻¹⁰, which can be regarded as extrinsic noise. We have created a stochastic simulation model based on the deterministic model¹⁹ that incorporated stochastic reactions due to the small number of molecules of the interval between PF and CF inputs²². We have previously shown that the spine uses probability of Ca^{2+} increase, rather than its amplitude, for information transfer, and that probability of Ca^{2+} increases in the spine shows robustness against input fluctuation, sensitivity to lower input numbers, and efficiency of information transfer²². However, the robustness, sensitivity and efficiency were not defined, and their mechanism remains unknown.

In this study, we made a simple stochastic model based on the simple deterministic model²⁰. Using the simple stochastic model, we defined the robustness, sensitivity and efficiency of information transfer by Ca^{2+} increase, and clarified their mechanisms (see Fig. 7). Furthermore, we found that the small-volume effect enables robust, sensitive and efficient information transfer in the spine volume, but not in the cell volume. We propose that the small-volume effect is one of the functional reasons why the spine has to be so small.

Results

Development of the simple stochastic model

To reduce complexity and computational cost of the detailed stochastic model (Fig. 1d)²², we constructed the simple stochastic model based on the simple deterministic model (Fig. 1e)²⁰. We set the parameters regarding to PF and CF inputs of simple deterministic model to reproduces the PF- and CF-timing dependent Ca^{2+} response of the detailed stochastic model²² (Fig. 1, Supplementary Fig. 1, Supplementary Table 1, 2, Method). Hereafter, we denoted $10^{-1} \mu\text{m}^3$ as the spine volume, and $10^3 \mu\text{m}^3$ as the cell volume. In the spine volume, coincident PF and CF inputs with $\Delta t = 100$ msec induced a large Ca^{2+} increase (Fig. 1f, red), but sometimes failed to induce a large Ca^{2+} increase (Fig. 1f, blue). We defined Ca_{res} as the temporal integration of Ca^{2+} concentration, subtracted by the basal Ca^{2+} concentration. The distribution of Ca_{res} showed a bimodal distribution (Fig. 1g). The distribution of Ca_{res} always showed a bimodal distribution regardless of the timing between PF and CF inputs, and probability of a large Ca^{2+} increase changed depending the timing between PF and CF inputs (Fig. 1h). We divided the distribution of Ca_{res} into the probability component (Fig. 1i) and the amplitude component (Fig. 1j) (see Methods). The probability component, but not the amplitude component, showed a bell-shaped time window, indicating that the timing information between PF and CF inputs is coded by the probability of large Ca^{2+} increase, rather than the amplitude of Ca^{2+} increase in the spine volume. By contrast, in the cell volume, the coincident PF and CF inputs with $\Delta t = 100$ msec always induced a large Ca^{2+} increase without failure (Fig. 1k) and Ca_{res} showed a unimodal distribution (Fig. 1l) (see Methods). The distribution of Ca_{res} always showed a unimodal distribution regardless of the timing between PF and CF inputs (Fig. 1m), and only the amplitude of Ca_{res} (Fig. 1o), but not the probability (Fig. 1n), showed a bell-shaped time window, indicating that the timing information between PF and CF inputs is coded by the amplitude of Ca^{2+} increase, rather than the probability of large Ca^{2+} increase in the cell volume. These results are consistent with our previous study using the detailed stochastic model²².

The simple stochastic model also showed the similar properties, such as efficiency, robustness, and sensitivity in the detailed stochastic model (Fig. 2, Supplementary Fig. 2). The mutual information between Ca_{res} and the PF- and CF-timing increased with the increase in the volume (Fig. 2a). In the spine volume, the probability component of the mutual information was larger than the amplitude component of the mutual information (Fig. 2a, inset), and the amplitude component of the mutual information became larger than the probability component of the mutual information with the increase in the volume. Mutual information per volume became the highest at the spine volume, and decreased with the increase in the volume (Fig. 2b), indicating that the most efficient information coding per volume is achieved at the spine volume. In the spine volume, the mutual information did not decrease and remained constant regardless of the CV (coefficient of variation) of PF input (Fig. 2c, black line), whereas that in the cell volume decreased with the increase in CV of PF input (Fig. 2c, yellow line, Supplementary Fig. 1), indicating that the information transfer by Ca_{res} is robust against

fluctuation of PF input only in the spine volume, but not in the larger volume including the cell volume. The detailed stochastic model showed a higher sensitivity to the lower numbers of PF input in the spine volume rather than the cell volume (Supplementary Fig. 2d)²². We showed that the higher sensitivity to low PF input can be seen in the spine volume, but not in the larger volume including the cell volume (see below). These results in the simple stochastic model are also consistent with those in the detailed stochastic model (Supplementary Fig. 2)²².

These results indicate that the simple stochastic model can retain the essential properties of Ca^{2+} response, such as robust, sensitive and efficient features. Using this simple stochastic model, we next defined the robustness, sensitivity, and efficiency, and clarified their mechanisms in the spine volume.

The mechanism of the robustness

In this section, we defined the robustness, and clarified the mechanism of the robustness as follows. The amplitudes of Ca^{2+} increase by conjunctive PF and CF inputs is compatible with those by strong PF input alone (see Supplementary Fig. 3k)¹⁹. Consistently, PF input alone has experimentally been shown to induce a large Ca^{2+} increase²³. Therefore, we hereafter used PF input alone. First, we showed that robustness is given by unchanging of the distribution of Ca_{res} against the fluctuation of PF input. We obtained the necessary and sufficient condition for the robustness, **that** the intrinsic noise is much larger than the extrinsic noise. We showed that the **range** of the fluctuation of PF input satisfying the conditions for the robustness is much larger in the spine volume than in the cell volume, indicating that the distribution of Ca_{res} against the fluctuation of PF input in the spine volume is more robust than the cell volume against the fluctuation of PF input.

Hereafter, for simplicity, we used only PF input alone instead of PF and CF inputs. The Amp_{PF} , amplitude of the PF input, was set to be between 150 and 215 unless otherwise noted. Consistently, PF input alone has experimentally been shown to induce a large Ca^{2+} increase²³. We performed the stochastic simulation 10^4 times per each amplitude of PF input, which is defined as Amp_{PF} , and obtained $p_c(\text{Ca}_{res}|\text{Amp}_{PF})$, the probability density distribution of Ca_{res} . Using $p_c(\text{Ca}_{res}|\text{Amp}_{PF})$, we examined the mechanism of the robustness. In the spine volume, the distribution of Ca_{res} , $p_c(\text{Ca}_{res}|\text{Amp}_{PF})$, became bimodal when Amp_{PF} exceeded around 50 (Fig. 3a, Supplementary Fig. 3a, b). By contrast, in the cell volume, the distribution of Ca_{res} always showed unimodal distribution regardless of Amp_{PF} , and its average monotonically increased along Amp_{PF} when Amp_{PF} exceeded around 150 (Fig. 3b, Supplementary Fig. 3i, j).

The robustness is given by unchanging of the distribution of Ca_{res} against the fluctuation of PF input

We have shown that the distribution of Ca_{res} for each Δt was unchanged regardless of CV of PF input in the spine volume, but not in the cell volume (see Supplementary Fig. 1)²², suggesting that unchanging of the distribution of Ca_{res} against the fluctuation of PF input is a key to the robustness of the information transfer. Therefore, we examined whether the distribution of Ca_{res} with PF input alone is also unchanged regardless of CV of PF input in the spine volume, but not in the cell volume.

Experimentally, it has been reported that the distribution of amplitude of PF input in the Purkinje cell can be approximated by a Gaussian distribution¹⁰. We set $p_c(Amp_{PF}|\mu_a, \sigma_a)$, the probability density distribution of Amp_{PF} , as the Gaussian distribution given by $\mathcal{N}(Amp_{PF}|\mu_a, \sigma_a^2)$, where μ_a and σ_a denote the average of Amp_{PF} and the standard deviation of Amp_{PF} , respectively. We used σ_a , the standard deviation of Amp_{PF} , as the magnitude of fluctuation of Amp_{PF} because the σ_a is proportional to CV_a , CV of Amp_{PF} , with the fixed μ_a , given by $CV_a = \sigma_a/\mu_a$. When PF input is given by $p_a(Amp_{PF}|\mu_a, \sigma_a)$, $p_{ac}(Ca_{res}|\mu_a, \sigma_a)$, the distribution of Ca_{res} with the fluctuation of Amp_{PF} , is given by

$$\begin{aligned} p_{ac}(Ca_{res}|\mu_a, \sigma_a) &= \int_{Amp_{PF}} p_a(a|\mu_a, \sigma_a) p_c(Ca_{res}|a) da \\ &= \int_{Amp_{PF}} \mathcal{N}(a|\mu_a, \sigma_a^2) p_c(Ca_{res}|a) da, \end{aligned} \quad (1)$$

where, $p_c(Ca_{res}|a)$ for each $a \in Amp_{PF}$, *i.e.* $p_c(Ca_{res}|Amp_{PF})$, was obtained by the stochastic simulation. In the spine volume, the distributions of Ca_{res} always exhibited the similar bimodal distributions regardless of CV_a and did not change even if the CV_a became larger (Fig. 3c–e). By contrast, in the cell volume, the distributions of Ca_{res} exhibited unimodal distribution with $CV_a = 0$, and with the increase in CV_a , the distributions of Ca_{res} changed and became bimodal (Fig. 3f–h). These properties remained the same regardless of the average of Amp_{PF} , μ_a (Supplementary Fig. 4). The similar results were obtained when both PF and CF inputs were used (see Supplementary Fig. 1).

Taken together, in the spine volume, the distribution of Ca_{res} remained almost unchanged against the fluctuation of Amp_{PF} , whereas, in the cell volume, the distribution of Ca_{res} largely varied against the fluctuation of Amp_{PF} . These results indicate that unchanging of the distribution of Ca_{res} against the fluctuation of Amp_{PF} causes the robustness.

We quantitated the change of the distributions of Ca_{res} with the increase in CV_a by the χ^2 distance against the distributions of Ca_{res} with $CV_a = 0$. The χ^2 distance becomes 0 when the distribution of Ca_{res} with a CV_a is the same with that with $CV_a = 0$, and the χ^2 distance becomes 1 when two distributions are completely different. In the spine volume, the χ^2 distance remained almost 0 regardless of CV_a , whereas, in the cell volume, the χ^2 distance abruptly increased with the increase in CV_a and became close to 1 (Fig. 3i), indicating that the distribution of Ca_{res} in the spine volume unchanges with

the increase in CV_a , whereas, that in the cell volume largely changes even with the small increase in CV_a . This is the reason why the robustness can be seen only in the spine volume but not in the cell volume.

The necessary and sufficient condition for the robustness

Next, we clarified the mechanism that the distribution of Ca_{res} in the spine volume unchanges with the increase in CV_a , whereas that in the cell volume largely changes even with the small increase in CV_a , and obtained the necessary and sufficient conditions for the robustness: unchanging of the distribution of the distribution of Ca_{res} regardless of CV_a . We considered $p_{ac}(Ca_{res}|\mu_a, \sigma_a)$, the distribution of Ca_{res} with the fluctuation of Amp_{PF} , with the increase in CV_a . Note that $CV_a = \sigma_a/\mu_a$. Since $\mathcal{N}(Amp_{PF}|\mu_a, \sigma_a^2)$ is symmetric with respect to the point μ_a , *i.e.* $\forall a \in Amp_{PF}$, $\mathcal{N}(a|\mu_a, \sigma_a^2) = \mathcal{N}(2\mu_a - a|\mu_a, \sigma_a^2)$, the equation (1) was deformed into

$$\begin{aligned}
p_{ac}(Ca_{res}|\mu_a, \sigma_a) &= \int_{\mu_a}^{\infty} \mathcal{N}(a|\mu_a, \sigma_a^2) p_c(Ca_{res}|a) da + \int_{-\infty}^{\mu_a} \mathcal{N}(a|\mu_a, \sigma_a^2) p_c(Ca_{res}|a) da \\
&= \int_{\mu_a}^{\infty} \mathcal{N}(a|\mu_a, \sigma_a^2) p_c(Ca_{res}|a) da + \int_{\mu_a}^{\infty} \mathcal{N}(2\mu_a - a|\mu_a, \sigma_a^2) p_c(Ca_{res}|2\mu_a - a) da \\
&= \int_{\mu_a}^{\infty} [\mathcal{N}(a|\mu_a, \sigma_a^2) p_c(Ca_{res}|a) + \mathcal{N}(a|\mu_a, \sigma_a^2) p_c(Ca_{res}|2\mu_a - a)] da \\
&= \int_{\mu_a}^{\infty} \mathcal{N}(a|\mu_a, \sigma_a^2) [p_c(Ca_{res}|a) + p_c(Ca_{res}|2\mu_a - a)] da. \tag{2}
\end{aligned}$$

Since the distribution of Amp_{PF} is the Gaussian distribution, $\mathcal{N}(Amp_{PF}|\mu_a, \sigma_a^2)$, the probability density that the $Amp_{PF} = a$ occurs decreases as the difference between a and μ_a becomes larger. In particular, the probability that $Amp_{PF} = a$ is included in the range $\mu_a - 3\sigma_a \leq a \leq \mu_a + 3\sigma_a$ is given by $\int_{\mu_a - 3\sigma_a}^{\mu_a + 3\sigma_a} \mathcal{N}(a|\mu_a, \sigma_a^2) da = 0.9974\dots$, *i.e.* almost 1. Thus, the probability of $a > \mu_a + 3\sigma_a$ or $a < \mu_a - 3\sigma_a$ is quite small and negligible. Therefore, satisfying the equation (2) in the range $\mu_a - 3\sigma_a \leq a \leq \mu_a + 3\sigma_a$ is enough to satisfy the equation (2) in almost all the range of Amp_{PF} . This means the r.h.s. (right-hand side) of the equation (2) in the range $a > \mu_a + 3\sigma_a$ can be neglected, and $p_{ac}(Ca_{res}|\mu_a, \sigma_a)$ is given by

$$p_{ac}(Ca_{res}|\mu_a, \sigma_a) = \int_{\mu_a}^{\mu_a + 3\sigma_a} \mathcal{N}(a|\mu_a, \sigma_a^2) [p_c(Ca_{res}|a) + p_c(Ca_{res}|2\mu_a - a)] da. \tag{3}$$

Here, we considered the two alternative cases. One is the case where the averaged distribution between the distributions of Ca_{res} with the $Amp_{PF} = a$ shifted $|a - \mu_a|$ from μ_a , the average of Amp_{PF} , *i.e.*, $1/2[p_c(Ca_{res}|a) + p_c(Ca_{res}|2\mu_a - a)]$, is almost the same as the distribution of Ca_{res} with $Amp_{PF} = \mu_a$, $p_c(Ca_{res}|\mu_a)$ up to $a = \mu_a + 3\sigma_a$, given by

$$\forall a < \mu_a + 3\sigma_a:$$

$$p_c(Ca_{res}|\mu_a) \simeq \frac{1}{2} [p_c(Ca_{res}|a) + p_c(Ca_{res}|2\mu_a - a)]. \quad (4)$$

The other is the case where the averaged distribution of Ca_{res} between the distributions of Ca_{res} with Amp_{PF} shifted $|a - \mu_a|$ from μ_a is not always the same as the distribution of Ca_{res} with μ_a up to $a = \mu_a + 3\sigma_a$, given by

$$\exists a < \mu_a + 3\sigma_a:$$

$$p_c(Ca_{res}|\mu_a) \neq \frac{1}{2} [p_c(Ca_{res}|a) + p_c(Ca_{res}|2\mu_a - a)]. \quad (5)$$

First, we considered the conditions where the equation (4) is satisfied, and obtained the condition where $p_{ac}(Ca_{res}|\mu_a, \sigma_a)$, the distribution of Ca_{res} with the fluctuation of Amp_{PF} , does not change against σ_a , the magnitude of fluctuation of Amp_{PF} . This condition means that the distribution of Ca_{res} remained the same against fluctuation of Amp_{PF} . Substituting the equation (4) for the equation (3), we obtained

$$\begin{aligned} p_{ac}(Ca_{res}|\mu_a, \sigma_a) &\simeq 2 \int_{\mu_a}^{\mu_a+3\sigma_a} \mathcal{N}(a|\mu_a, \sigma_a^2) p_c(Ca_{res}|\mu_a) da \\ &= 2p_c(Ca_{res}|\mu_a) \int_{\mu_a}^{\mu_a+3\sigma_a} \mathcal{N}(a|\mu_a, \sigma_a^2) da \\ &\simeq p_c(Ca_{res}|\mu_a). \end{aligned} \quad (6)$$

The l.h.s. (left-hand side) of the equation (6) indicates the distribution of Ca_{res} with the fluctuation of Amp_{PF} . The l.h.s. is almost the same as the r.h.s. that indicates the distribution of Ca_{res} without the fluctuation of Amp_{PF} . Note that the σ_a does not directly appear in the equation (4), however, σ_a determines the upper bound of the range of $a - \mu_a$ satisfying the equation (4). This means that if the equation (6) is satisfied for $\sigma_a = \sigma_a^*$, the equation (6) is also satisfied for $\sigma_a < \sigma_a^*$. Namely, the upper bound of the range of $a - \mu_a$ satisfying the equation (4) is larger, the equation (6) is satisfied for larger σ_a , *i.e.* CV_a . Therefore, the equation (4) is the condition sufficient to allow that the distribution of Ca_{res} does not change against the fluctuation of Amp_{PF} .

By contrast, under the conditions where the equation (5) is satisfied, there does not exist $p_{ac}(Ca_{res}|\mu_a, \sigma_a)$, the distribution of Ca_{res} with the fluctuation of Amp_{PF} , which does not change against the fluctuation of Amp_{PF} (see Supplementary Note 1).

Taken together, the equation (4) is a necessary and sufficient condition where the distribution of Ca_{res} remains the same against the fluctuation of Amp_{PF} . If $a - \mu_a$, the effective Amp_{PF} with the fluctuation of Amp_{PF} , satisfying the equation (4) is larger, the distribution of Ca_{res} does not change even against the larger fluctuation of Amp_{PF} . Therefore, the upper bound

of the range of $a - \mu_a$ satisfying the equation (4) determines the maximum of σ_a where the distribution of Ca_{res} does not change. Next, we examined the upper bounds of the range of $a - \mu_a$ satisfying the equation (4) in the spine volume and in the cell volume. We also demonstrated that the upper bound of the range of $a - \mu_a$ satisfying the equation (4) in the spine volume is much larger than that in the cell volume, thus, information transfer by Ca_{res} in the spine volume is much more robust than that in the cell volume against the fluctuation of Amp_{PF} .

The necessary and sufficient condition for the robustness is satisfied in the range where the intrinsic noise is larger than the extrinsic noise

We next showed that the upper bound of the range of Amp_{PF} satisfying the equation (4) is determined by the upper bound of the range of Amp_{PF} where the intrinsic noise is larger than the extrinsic noise. We first gave the intuitive interpretation of this proposition using schematic representation of the distribution of Ca_{res} with indicated Amp_{PF} in the spine volume and cell volume (Fig. 3j, Supplementary Fig. 3) and then proved it. The distribution of Ca_{res} in the spine volume is divided into two distributions by threshold θ (Fig. 3j, see Supplementary Fig. 3). Note that because of the unimodal distribution of Ca_{res} in the cell volume, we set $\theta = -\infty$ in the cell volume. This means that the equation (4) was divided into the forms given by

$$p_c(Ca_{res}|Amp_{PF}) = P_+(Amp_{PF})p_c(Ca_{res}|Ca_{res} > \theta, Amp_{PF}) + P_-(Amp_{PF})p_c(Ca_{res}|Ca_{res} \leq \theta, Amp_{PF}), \quad (7)$$

$$\begin{cases} P_+(Amp_{PF}) \equiv \int_{\theta}^{\infty} p_c(c|Amp_{PF}) dc \\ P_-(Amp_{PF}) \equiv \int_{-\infty}^{\theta} p_c(c|Amp_{PF}) dc \end{cases}, \quad (8)$$

where P_+ and P_- denote the probabilities of $Ca_{res} > \theta$ and $Ca_{res} \leq \theta$ with $Amp_{PF} = a$, respectively. We separately considered the first term and second term of r.h.s. It should be noted that since θ in the cell volume was set at $-\infty$, P_+ in the cell volume is always 1 for any Amp_{PF} . Furthermore, we defined $Amp'_{PF} \equiv Amp_{PF} - \mu_a$, the relative amplitude of PF input, as the difference of Amp_{PF} from μ_a , the average of Amp_{PF} . $\hat{p}_c(Ca_{res}|x)$, the distribution of Ca_{res} with $Amp'_{PF} = x$, was defined from $p_c(Ca_{res}|a)$, the distribution of Ca_{res} with $Amp_{PF} = a$, given by

$$\hat{p}_c(Ca_{res}|x) \equiv p_c(Ca_{res}|\mu_a + x) = p_c(Ca_{res}|a) \quad (9)$$

Then, the equations (4) and (7) were deformed, respectively, given by

$$\hat{p}_c(Ca_{res}|0) = \frac{1}{2}[\hat{p}_c(Ca_{res}|x) + \hat{p}_c(Ca_{res}|-x)], \quad (10)$$

$$\hat{p}_c(Ca_{res}|x) = P_+(\mu_a + x)\hat{p}_c(Ca_{res}|Ca_{res} > \theta, x) + P_-(\mu_a + x)\hat{p}_c(Ca_{res}|Ca_{res} \leq \theta, x). \quad (11)$$

In the spine volume, the distributions of Ca_{res} above the threshold θ with $Amp'_{PF} = x$ (Fig. 3j, blue in the left panel, blue line) and with $Amp'_{PF} = -x$ (Fig. 3j, the left panel, the red line) had $\sigma_c(\mu_a \pm x)$, the standard deviation of Ca_{res} , which is larger than ΔCa^* , the gap of the Ca_{res} realizing the peaks of distributions of Ca_{res} , and these distributions widely overlapped each other. Then, the averaged distribution of these two distributions of Ca_{res} with $Amp'_{PF} = \pm x$ became the unimodal and intermediate distribution (Fig. 3j, the left panel, the green dashed line), and became almost the same as the distribution of Ca_{res} above threshold θ with $Amp'_{PF} = 0$ (Fig. 3j, black line in the left panel, the black line). Also, the distributions of Ca_{res} below the threshold θ exhibited the similar unimodal distribution. Thus, the averaged distribution of these two distributions below the threshold θ (Fig. 3j, the left panel, the green dashed line) became almost the same as the distribution of Ca_{res} below the threshold θ with $Amp'_{PF} = 0$ (Fig. 3j, the left panel, the black line). Therefore, in the spine volume, for the both distributions of Ca_{res} above and below the threshold θ , the averaged distributions of the distributions of Ca_{res} with $Amp'_{PF} = \pm x$ were the same as that with $Amp'_{PF} = 0$, indicating that the equation (4) is satisfied. This also means that any symmetrical distribution of Amp'_{PF} other than the Gaussian distribution can give the same result. By contrast, in the cell volume, the distributions of Ca_{res} with $Amp'_{PF} = x$ (Fig. 3j, the right panel, the red line) and $Amp'_{PF} = -x$ (Fig. 3j, the right panel, the blue line) had the standard deviations which are smaller than ΔCa^* , the gap of the Ca_{res} realizing the peaks of distributions of Ca_{res} , and did not overlapped each other. Then, the averaged distribution of these two distributions (Fig. 3j, the right panel, the green dashed line) became bimodal and did not conform to the distribution of Ca_{res} with $Amp'_{PF} = 0$ (Fig. 3j, the right panel, the black line), indicating that the equation (4) is not satisfied. Therefore, the symmetry of the distribution of Amp'_{PF} and large σ_c , the standard deviations of the distribution of Ca_{res} , in comparison to ΔCa^* , the gap of the Ca_{res} realizing peaks of distributions of Ca_{res} , can give the conformation of the averaged distribution of the two distributions of Ca_{res} with $Amp'_{PF} = \pm x$ to the distribution with $Amp'_{PF} = 0$. Then, we proved this proposition. For this purpose, we derived the upper bound of the range of x where the equation (4) is satisfied, and showed that this upper bound in the spine volume is larger than that in the cell volume.

We tried to examine the upper bound of the range of x where the equation (4) is satisfied, and showed that the upper bound of the range of x in the spine volume is larger than that in the cell volume. Hereafter, each distribution of Ca_{res} for $Ca_{res} > \theta$ and $Ca_{res} \leq \theta$ is approximated by the Gaussian distribution. We tried to examine that the equation (4) is satisfied when σ_c , the standard deviation of Ca_{res} , is larger than ΔCa^* , the gap of Ca^* with $Amp'_{PF} = x$ and $Amp'_{PF} = -x$.

Here, we considered the small gap of Amp'_{PF} , hence, for simplicity, $\sigma_c(\mu_a + x)$ and $\sigma_c(\mu_a - x)$, the standard deviations of Ca_{res} with $Amp_{PF} = \mu_a + x$ and $Amp'_{PF} = \mu_a - x$, were regarded as $\sigma_c(\mu_a)$, the standard deviation of Ca_{res} with $Amp_{PF} = \mu_a$, up to the upper bound of the range of x satisfying the equation (4) (Supplementary Fig. 5).

First, we considered $\hat{p}_c(Ca_{res}|Ca_{res} > \theta, x)$, the distribution of Ca_{res} , for $Ca_{res} > \theta$ in the spine and cell volumes, we approximated the distribution of Ca_{res} for $Ca_{res} > \theta$ by the Gaussian distribution, given by

$$\hat{p}_c(Ca_{res}|Ca_{res} > \theta, x) \simeq \frac{1}{\sqrt{2\pi\sigma_c^2}} \exp\left[-\frac{(Ca_{res} - Ca^*(\mu_a + x))^2}{2\sigma_c^2}\right]. \quad (12)$$

Ca^* indicates the Ca_{res} realizing the peak of distribution of Ca_{res} , given by

$$Ca^*(a) = \arg \max_{Ca_{res}} p_c(Ca_{res}|Ca_{res} > \theta, a). \quad (13)$$

As mentioned above, we assumed $\sigma_c \equiv \sigma_c(\mu_a \pm x) = \sigma_c(\mu_a)$.

Then, for $Ca_{res} > \theta$, we substituted the equations (11) and (12) into the r.h.s. of the equation (10), and obtained

$$\begin{aligned} & \frac{1}{2} [\hat{p}_c(Ca_{res}|x) + \hat{p}_c(Ca_{res}|-x)] \\ & \simeq \frac{1}{2} \left\{ \frac{P_+(\mu_a + x)}{\sqrt{2\pi\sigma_c^2}} \exp\left[-\frac{(Ca_{res} - Ca^*(\mu_a + x))^2}{2\sigma_c^2}\right] + \frac{P_+(\mu_a - x)}{\sqrt{2\pi\sigma_c^2}} \exp\left[-\frac{(Ca_{res} - Ca^*(\mu_a - x))^2}{2\sigma_c^2}\right] \right\}. \end{aligned} \quad (14)$$

Here, we considered Ca^* . Ca^* for $Ca_{res} > \theta$ linearly increased from around $Amp_{PF} = 50$ in the spine volume (Fig. 4a, black line). In the spine volume, Ca^* for $Ca_{res} > \theta$ linearly increased with the increase in Amp_{PF} for $150 \leq Amp_{PF} \leq 215$, which corresponds to the range of the PF and CF input timing. Thus, regarding Ca^* for $Ca_{res} > \theta$, we could assume

$$Ca^*(\mu_a \pm x) \simeq Ca^*(\mu_a) \pm \Delta Ca^*(x). \quad (15)$$

Equation (15) indicates that the difference of Ca^* between with $Amp_{PF} = \mu_a + x$ and with $Amp_{PF} = \mu_a$ is the same as that between with $Amp_{PF} = \mu_a$ and with $Amp_{PF} = \mu_a - x$, where ΔCa^* indicates the difference of Ca^* between with $Amp_{PF} = \mu_a \pm x$ and with $Amp_{PF} = \mu_a$. By contrast to the spine volume, in the cell volume, Ca^* abruptly arose at $Amp_{PF} = 150$, and gradually increased with the increase in Amp_{PF} (Fig. 4a, yellow line). Therefore, in the cell volume, the equation (15) is not satisfied around $Amp_{PF} = 150$, but almost satisfied for $150 < Amp_{PF} \leq 215$. Then, we substituted the equation (15) into the equation (14), and obtained

$$\begin{aligned}
&\simeq \frac{1}{2} \left\{ \frac{P_+(\mu_a + x)}{\sqrt{2\pi\sigma_c^2}} \exp \left[-\frac{(Ca_{res} - Ca^*(\mu_a) - \Delta Ca^*(x))^2}{2\sigma_c^2} \right] \right. \\
&\quad \left. + \frac{P_+(\mu_a - x)}{\sqrt{2\pi\sigma_c^2}} \exp \left[-\frac{(Ca_{res} - Ca^*(\mu_a) + \Delta Ca^*(x))^2}{2\sigma_c^2} \right] \right\} \\
&= \frac{1}{2\sqrt{2\pi\sigma_c^2}} \exp \left[-\frac{(Ca_{res} - Ca^*(\mu_a))^2}{2\sigma_c^2} \right] \exp \left[-\frac{\Delta Ca^*(x)^2}{2\sigma_c^2} \right] \\
&\times \left\{ P_+(\mu_a + x) \exp \left[\frac{(Ca_{res} - Ca^*(\mu_a))\Delta Ca^*(x)}{\sigma_c^2} \right] + P_+(\mu_a - x) \exp \left[-\frac{(Ca_{res} - Ca^*(\mu_a))\Delta Ca^*(x)}{\sigma_c^2} \right] \right\}. \quad (16)
\end{aligned}$$

Here, we considered the range of Ca_{res} where $|Ca_{res} - Ca^*(x)| \leq 3\sigma_c(x)$ is almost satisfied. Hence, if $\Delta Ca^*(x) \ll \sigma_c(x)$, then, we could approximate

$$\simeq \frac{1}{\sqrt{2\pi\sigma_c^2}} \exp \left[-\frac{(Ca_{res} - Ca^*(\mu_a))^2}{2\sigma_c^2} \right] \left\{ \frac{P_+(\mu_a + x) + P_+(\mu_a - x)}{2} \right\}. \quad (17)$$

Note that, as mentioned below, the upper bound of the range of x where $\Delta Ca^* \ll \sigma_c$ determines the upper bound of the range where the equation (4) is satisfied. This means that the larger upper bound of the range of x where $\Delta Ca^* \ll \sigma_c$ corresponds to the maximum of CV_a with which the distribution of Ca_{res} does not change.

Here, we considered the probability that Ca_{res} exceeds the threshold θ , P_+ . In the spine volume, P_+ gradually arose from $Amp_{PF} = 50$, linearly increased for $100 \leq Amp_{PF} \leq 250$ (Fig. 4b, black line). Therefore, in the spine volume, P_+ linearly increased with the increase in Amp_{PF} for $150 \leq Amp_{PF} \leq 215$, which corresponds to the range of the PF-CF input timing. Thus, regarding P_+ , we could assume

$$\frac{1}{2} [P_+(\mu_a + x) + P_+(\mu_a - x)] = P_+(\mu_a). \quad (18)$$

This equation indicates that the average of the probabilities that Ca_{res} exceeds the threshold θ with $Amp_{PF} = \mu_a + x$ and $Amp_{PF} = \mu_a - x$ is the same as the probability that Ca_{res} exceeds the threshold θ with $Amp_{PF} = \mu_a$. In the cell volume, the distribution of Ca_{res} was unimodal, and $\theta = -\infty$ was assumed, then, P_+ was always 1, and the equation (18) was always satisfied. Therefore, we substituted the equation (18) into the equation (17), and obtained

$$\simeq \frac{P_+(\mu_a)}{\sqrt{2\pi\sigma_c^2}} \exp \left[-\frac{(Ca_{res} - Ca^*(\mu_a))^2}{2\sigma_c^2} \right] = \hat{p}_c(Ca_{res}|0). \quad (19)$$

for $Ca_{res} > \theta$, *i.e.* the equation (4) for $Ca_{res} > \theta$ is satisfied.

On the other hand, for $Ca_{res} \leq \theta$, because Ca^* for $Ca_{res} \leq \theta$ was almost constant, the distribution Ca_{res} was mainly characterized only by P_- of the distribution of Ca_{res} , indicating

$$\hat{p}_c(Ca_{res}|Ca_{res} \leq \theta, 0) = \hat{p}_c(Ca_{res}|Ca_{res} \leq \theta, \pm x). \quad (20)$$

Then, using the equation (4) for $Ca_{res} \leq \theta$, similar to the case for $Ca_{res} > \theta$, we obtained

$$\begin{aligned} \hat{p}_c(Ca_{res}|, 0) &= P(0)\hat{p}_c(Ca_{res}|Ca_{res} \leq \theta, 0) \\ &\simeq \frac{1}{2}[P_-(x) + P_-(-x)]\hat{p}_c(Ca_{res}|Ca_{res} \leq \theta, 0) \\ &= \frac{1}{2}[P_-(x)\hat{p}_c(Ca_{res}|Ca_{res} \leq \theta, 0) + P_-(-x)\hat{p}_c(Ca_{res}|Ca_{res} \leq \theta, 0)] \\ &= \frac{1}{2}[P_-(x)\hat{p}_c(Ca_{res}|Ca_{res} \leq \theta, x) + P_-(-x)\hat{p}_c(Ca_{res}|Ca_{res} \leq \theta, -x)] \\ &= \frac{1}{2}[\hat{p}_c(Ca_{res}|x) + \hat{p}_c(Ca_{res}|, -x)] \end{aligned} \quad (21)$$

for $Ca_{res} \leq \theta$, *i.e.* the equation (4) for $Ca_{res} \leq \theta$ is also satisfied. Therefore, from the equations (19) and (21), we derived the equation (4). Thus, we approximately showed that if Ca^* and P_+ , linearly increase with the increase in Amp_{PF} and $\Delta Ca^* \ll \sigma_c$, the equation (4) was satisfied. This means that the necessary and sufficient condition for the robustness is satisfied in the range where the intrinsic noise, σ_c , is larger than the extrinsic noise, ΔCa^* .

The range of the fluctuation of PF input satisfying the conditions for the robustness is larger in the spine volume than in the cell volume

We next examined the range of the fluctuation of PF input satisfying the condition for the robustness. In the spine volume, in the range considered ($150 \leq Amp_{PF} \leq 215$), $Ca^*(x)$ and P_+ always linearly increase with the increase in Amp_{PF} . Thus, the range of Amp_{PF} where the distribution of Ca_{res} remains the same regardless of CV_a in the spine volume was determined by the range satisfying $\Delta Ca^* \ll \sigma_c$. In the spine volume, $\Delta Ca^*/\sigma_c \ll 1$ when x was small, $\Delta Ca^*/\sigma_c$ increased with the increase in x , and exceeded 1 at $x = 110$ (Fig. 4c). By contrast, in the cell volume, $\Delta Ca^*/\sigma_c$ exceeded 1 even at $x = 2$ (Fig. 4d). We defined δ_{max} as x that gives $\Delta Ca^*/\sigma_c = 1$. δ_{max} relatively provides the upper bound of x where $\Delta Ca^*/\sigma_c \ll 1$. Thus, we used δ_{max} as the index of the robustness (Fig. 4e). The larger δ_{max} means the more robustness. δ_{max} was the highest at the spine volume and decreased with the increase in volume (Fig. 4e), indicating that the spine volume gives the highest robustness. Since δ_{max} in the spine volume was much larger than that in the cell volume, the upper bound of x where $\Delta Ca^*/\sigma_c \ll 1$ in the spine volume is much larger than that in the cell volume. Here, x denoted the relative amplitude of PF input as the displacement of Amp_{PF} from average of Amp_{PF} , μ_a , given by $Amp'_{PF} = Amp_{PF} - \mu_a$, *i.e.* larger x corresponds to larger CV_a . Therefore, in the spine volume, in the range $150 < Amp_{PF} \leq 215$, since $\Delta Ca^*/\sigma_c$ was smaller

than 1 even with larger x , information transfer by Ca_{res} is robust with larger CV_a . By contrast, in the cell volume, since $\Delta Ca^*/\sigma_c$ was larger than 1 even with small x , information transfer by Ca_{res} is not robust even with small CV_a .

Next, we confirmed that, when $\Delta Ca^*/\sigma_c$ is small than 1, the distribution of Ca_{res} with $Amp_{PF} = \mu_a$ and the averaged distribution of Ca_{res} for $Amp_{PF} = \mu_a \pm x$ becomes the same. We quantified the similarities between the two distributions of Ca_{res} by the χ^2 distance. In the spine volume (Fig. 4f, red), most of $\Delta Ca^*/\sigma_c$ were smaller than 1, and the χ^2 distance were also small, indicating that $\Delta Ca^*/\sigma_c$ was smaller than 1 and the two distributions of Ca_{res} were quite similar in the spine volume. By contrast, in the cell volume (Fig. 4f, blue), most of $\Delta Ca^*/\sigma_c$ were larger than 1, and the χ^2 distance were almost 1 indicating that $\Delta Ca^*/\sigma_c$ was larger than 1, and the two distributions of Ca_{res} were quite different. Therefore, when ΔCa^* , the gap of two distributions of Ca_{res} , is smaller than σ_c , the standard deviation of the distribution of Ca_{res} , the distribution of Ca_{res} unchanges and becomes robust against fluctuation of PF input.

In summary, in the spine volume, σ_c , the standard deviation of the distribution of Ca_{res} , is larger than ΔCa^* , the gap of the Ca_{res} realizing the peaks of distributions of Ca_{res} , that reflects the fluctuation of Amp_{PF} , indicating that the range of x satisfying $\Delta Ca^* \ll \sigma_c$ is wider. This means that the distribution of Ca_{res} with fluctuation of amplitude of PF input conforms to that without fluctuation of amplitude of PF input. Moreover, $\Delta Ca^* \ll \sigma_c$ indicates that the gap of distribution Ca_{res} caused by extrinsic noise, ΔCa^* , is much smaller than that caused by intrinsic noise, σ_c . Hence, the information transfer by Ca_{res} becomes robust against fluctuation of amplitude of PF input. By contrast, in the cell volume, the standard deviation of the distribution of Ca_{res} without fluctuation of amplitude of PF input is small, and the averaged distribution of Ca_{res} with fluctuation of amplitude of PF input does not conform to that without fluctuation of amplitude of PF input. Moreover, $\Delta Ca^* > \sigma_c$ indicates that the gap of distribution of Ca_{res} caused by extrinsic noise, ΔCa^* , is larger than that caused by intrinsic noise, σ_c . Hence, the information transfer by Ca_{res} is not robust against fluctuation of amplitude of PF input.

The mechanism of the sensitivity

In the detailed stochastic model, the Ca^{2+} response was sensitive to lower numbers of PF inputs in the spine volume than the cell volume²². We tried to examine the sensitivity in the simple stochastic model, and defined the ‘‘sensitivity’’ as follows. For each volume, the PF input was given by the Gaussian distribution with the fixed standard deviation, and the average amplitude of PF input was varied (see Methods). The average amplitude, μ_s , giving the maximum of mutual information, Amp^* , was defined as an index of sensitivity for each volume. Smaller Amp^* indicates higher sensitivity to lower amplitude of PF input.

In the spine volume, the mutual information exhibited the bell-shaped response where $Amp^* = 100$ gives the maximum mutual information (Fig. 5a, black line and the white triangle, Fig. 5b, Supplementary Fig. 6a, f). With the increase in volume, Amp^* shifted to around 220 (Fig. 5a, orange line and the black triangle, Fig. 5b, Supplementary Fig. 6e, j). This result indicates that the spine volume shows the higher sensitivity to the lower amplitude of PF input than larger volume including the cell volume.

We considered the mechanism that the spine shows the higher sensitivity to the lower amplitude of PF input. When the standard deviation of PF input distribution is the same, the mutual information depends on ΔCa_{STD}^* , the dynamic range of the output, and σ_c , the standard deviation of the output (Supplementary Fig. 7). For example, when the dynamic range of the output is the same, the smaller standard deviation of the output gives the higher mutual information. When the standard deviation of the output is the same, the broader dynamic range gives the higher mutual information. For simplicity, the window width of the input distribution of Amp_{PF} was set as the finite range defined as the average \pm standard deviation of the input distribution of Amp_{PF} , *i.e.* $\mu_s \pm STD$, and the dynamic range was denoted as the gap of Ca_{res} realizing peaks of distributions of Ca_{res} between upper bound ($Amp_{PF} = \mu_s + STD$) and lower bound ($Amp_{PF} = \mu_s - STD$) of the input distribution of Amp_{PF} , *i.e.* $\Delta Ca_{STD}^* = Ca^*(\mu_s + STD) - Ca^*(\mu_s - STD)$.

First we considered ΔCa_{STD}^* , the dynamic range of the output. We defined $\psi(V)$ for each volume as Amp_{PF} where the Ca^* begins to increase (Supplementary Fig. 8a). In the spine volume, Ca^* linearly increased along Amp_{PF} for $Amp_{PF} > \psi(V)$ (Fig. 4a, Supplementary Fig. 8a), hence, ΔCa_{STD}^* was largely variable and independent of Amp_{PF} (Fig. 5c, Supplementary Fig. 8b, e–h). By contrast, in the cell volume, ΔCa_{STD}^* was bell-shaped curve with the maximum at $Amp_{PF} = 200$ (Fig. 5d, Supplementary Fig. 8c, u–x).

Next, we considered σ_c , the standard deviation of Ca_{res} for $Ca_{res} > \theta$. In the spine volume, σ_c gradually increased with the increase in Amp_{PF} for $Amp_{PF} > \psi(10^{-1}) \simeq 50$ (Fig. 5c, blue line). By contrast, in the cell volume, σ_c became largest around $Amp_{PF} = 150$ and gradually decrease with the increase in Amp_{PF} (Fig. 5d, blue line).

In the spine volume, ΔCa_{STD}^* was almost constant for $Amp_{PF} > 60$ and σ_c increased along Amp_{PF} , and therefore, the mutual information became maximum around $Amp_{PF} = 60$ (see Supplementary Fig. 8e–h, black dashed line, also see Supplementary Fig. 6a, f). By contrast, in the cell volume, the mutual information became maximum at $Amp_{PF} = 235$, which is greater than $Amp_{PF} = 200$ giving the maximum of ΔCa_{STD}^* (Fig. 5a, d, see Supplementary Fig. 8u–x, black dashed line, also see Supplementary Fig. 6e, j). This is because despite the higher ΔCa_{STD}^* , σ_c was larger and the loss of information became large. Decreasing σ_c resulted in increase of mutual information.

Thus, the mutual information becomes the maximum at $Amp_{PF} = 60$ in the spine volume and at $Amp_{PF} = 250$ in the cell volume, indicating the higher sensitivity to lower amplitude of PF input in the spine volume.

The mechanism of the efficiency

We defined the efficiency as the mutual information per PF input. The average of PF input was given by $\mu_s \times V$, whose dimension is equal to number of molecule. The efficiency means how much information can be transferred by a unitary PF input. The higher mutual information per PF input indicates the higher efficiency. The mutual information monotonically increased with the increase in volume, and the rate of the increase of the mutual information decreased with the increase in volume (Fig. 6a, black) and therefore, the mutual information per PF input monotonically decreased (Fig. 6b, black line), indicating that the mutual information per PF input, *i.e.* the efficiency, was larger in the spine volume, and decreased as the volume increased to the cell volume (Fig. 6b, black line).

Next, we examined the mechanism of the volume-dependency of the mutual information. The slope of the mutual information decreased with the increase in volume, and became close to logarithmic increase in the larger volume (Fig. 6a, black). Then, we assumed that the volume-dependent increase of the mutual information is roughly approximated with constants, a, b, c (Methods), as given by

$$I(Ca_{res}; \Delta t) \approx a \log_2(b + c \cdot V). \quad (22)$$

This function fitted well the volume-dependent mutual information (Fig. 6a, red line) and the mutual information per PF input (Fig. 6b, red line), indicating that this function captures the features of the volume-dependency of the mutual information in the spine volume and the larger volume.

We also considered the Gaussian channel, simple linear transmission system. For the input X , when the system noise Z obeys the Gaussian distribution, the output $Y = X + Z$ also obeys the Gaussian distribution. In this case, under the constraint $E[X^2] < F$, the mutual information (channel capacity) between the input, X , and the output, Y , is simply described as

$$I(Y; X) = \frac{1}{2} \log_2 \left(1 + \frac{F}{\sigma_Z^2} \right), \quad (23)$$

where, F denotes the power constraint of input, and σ_Z denotes the standard deviation of the noise intensity. Here, F is regarded as a constant value because the input distribution for calculating $I(Ca_{res}; \Delta t)$ in the equation (22) (Fig. 6, blue line) is assumed to be unchanged. It has been shown that the standard deviation of reactions is proportional to the power of number of the molecules, *i.e.* volume, so that the fluctuation of number of molecules can be approximated as $\sigma_Z'^2 \propto V^{24}$.

Then, the fluctuation of concentration of molecules can be approximated by $\sigma_z^2 = (\sigma_z'/V)^2 \propto V^{-1}$. Therefore, the mutual information for the Gaussian channel is given by

$$I(Ca_{res}; \Delta t) \approx \frac{1}{2} \log_2(1 + c \cdot V) \quad (24)$$

(Fig. 6a, b, blue lines). Equations (22) and (24) indicates the same volume-dependency of the mutual information. However, in the smaller volume including the spine volume, the mutual information per PF input of the Ca^{2+} response was larger than that of the Gaussian channel and the fitted function (Fig. 6b). This difference in volume-dependency is likely to be caused by the different values of the parameters $a = 0.3924651$ and $c = 0.5128671$, which were larger than 1/2 and 1 in the fitted function and equal in the Gaussian channel, respectively. There were other differences in both systems; the noise of the system in this study is not exactly a Gaussian noise, and the input-output relation is nonlinear. Despite such differences, both systems exhibited the similar volume-dependency of the mutual information, suggesting that the more efficient information transfer in the smaller volume is a universal property in the general information transduction systems.

Discussion

In this study, we made the simple stochastic model of Ca^{2+} increase in the spine of PF-cerebellar Purkinje cell synapse. We clarified the mechanisms of the robustness, sensitivity, and efficiency, and showed that these properties become prominent in the spine volume (Fig. 7). The robustness appears under the condition where the standard deviation of the distribution of the Ca^{2+} response, intrinsic noise, is larger than the fluctuation of the distribution of the Ca^{2+} response caused by the PF input fluctuation, extrinsic noise.

The higher sensitivity to the lower amplitude of PF input requires the wider dynamic range of Ca^{2+} response and the smaller standard deviation of the distribution of Ca^{2+} response in the range of the lower amplitude of PF input. In the spine volume, because of the stochastic facilitation caused by the stochasticity in reactions²⁵, even the weak PF input can induce a large Ca^{2+} increase, resulting in a wider dynamic range of Ca^{2+} response in the range of the lower amplitude of PF input in the spine volume than in the cell volume. Moreover, the standard deviation of the distribution of the Ca^{2+} response in the range of the lower amplitude of PF input was small. In the larger volume than the spine volume, the sensitivity abruptly decreases because stronger PF input was required for compensating the large standard deviation of the distribution of Ca^{2+} response.

The highest efficiency in the spine volume is derived from the nature of the volume-dependency of mutual information; the rate of increase of the mutual information monotonically decreased with the increase in volume. Then, the mutual

information per PF input, efficiency, becomes larger in the smaller volume. This result indicates that the spine utilizes the limit of the smallness to acquire the highest efficiency.

Robustness appears when intrinsic noise is larger than extrinsic noise. Sensitivity appears because of the stochastic facilitation. Efficiency appears because of the nature of volume-dependency of information transfer. These characteristics are derived from the smallness, which we denote “the small-volume effect”. The small-volume effect enables the spine robust, sensitive and efficient information transfer. The small-volume effect may be seen not only in spines, but also in other small intracellular organelles, and general strategy for biological information transfer. The small-volume effect is one of the reasons why the spine has to be so small. The small-volume effect is also equivalent to the small-number effect, suggesting that the robustness, sensitivity, and efficiency can also be seen under the conditions where numbers of molecules are limited even in a larger volume.

It has been known that in most of the excitable neurons, the Ca^{2+} increase in the spine by the glutamine stimulus depends mainly on NMDAR, another glutamate-gated Ca^{2+} channel^{26–28}. In the future, we will analyze whether the Ca^{2+} increase by NMDAR in the spine also shows the robustness, sensitivity and efficiency and ask whether such properties are conserved among the spines regardless of the types of the receptors.

Methods

Simple stochastic model

The block diagram of the simple stochastic model is the same as that of the simple deterministic model (Fig. 1e)¹. The inputs are PF and CF . After the Fig. 3 unless specified in Fig. 6, we set $CF = 0$, and used only PF as the input. The output is Ca .

The total cytosolic Ca^{2+} in the spine of the Purkinje cell, Ca , is derived from the three pathways.

$$Ca = Ca_{basal} + Ca_{VGCC} + Ca_{IP_3}. \quad (25)$$

where Ca_{basal} , Ca_{VGCC} and Ca_{IP_3} denote the basal cytosolic Ca^{2+} , Ca^{2+} through voltage-gated Ca^{2+} channel (VGCC) triggered by CF , and through IP_3 receptors of the internal Ca^{2+} store triggered by PF , respectively. Ca_{basal} is constantly produced and described by

$$\phi \xrightarrow{C_b/\tau_{FB}} Ca_{basal} \xrightarrow{1/\tau_{FB}} \phi, \quad (26)$$

where C_b/τ_{FB} and $1/\tau_{FB}$ denote the production and decay rate constants of Ca_{basal} , respectively. Hereafter, ϕ denotes a fixed value.

Ca_{VGCC} is triggered by CF , and described by

$$CF \xrightarrow{1/\tau_{CF}} Ca_{VGCC} \xrightarrow{1/\tau_{CF}} \phi, \quad (27)$$

where $1/\tau_{CF}$ denotes the production and decay rate constants of Ca_{VGCC} , respectively. CF is given by $Amp_{CF} \cdot V$ at $t = t_{CF}$.

Ca_{IP_3} is produced as follows. Briefly, PF produces IP_3 . Ca has a positive feedback (FB) through the activation of IP_3 receptor (G_{IP_3R}). IP_3 and G_{IP_3R} synergistically induce Ca release through IP_3R (Ca_{IP_3}). IP_3 is triggered by PF , and described by

$$PF \xrightarrow{1/\tau_{PF}} IP_3 \xrightarrow{1/\tau_{PF}} \phi, \quad (28)$$

where $1/\tau_{PF}$ denotes the production and decay rate constants of IP_3 . PF is given by $Amp_{PF} \cdot V$ at $t = t_{PF}$.

The time-delay variable FB is described by

$$Ca \xrightarrow{1/\tau_{FB}} FB \xrightarrow{1/\tau_{FB}} \phi, \quad (29)$$

where $1/\tau_{FB}$ denotes the production and decay rate constants of FB . This decay rate constant also determines the degradation rate of Ca_{IP_3} .

IP_3 receptor coupled with Ca^{2+} , G_{IP_3R} , is mediated by the positive and negative feedbacks from FB , and is given by the nonlinear function, described by

$$G_{IP_3R} = Amp_{G_{IP_3R}} \left\{ \frac{k \cdot FB}{(k + FB)(K + FB)} \right\}^{n_{G_{IP_3R}}}, \quad (30)$$

where $Amp_{G_{IP_3R}}$, k , K and $n_{G_{IP_3R}}$ denote the amplitude of feedback, thresholds of FB for the positive and negative feedbacks, and non-linearity of feedback, respectively.

Ca released from IP_3R , Ca_{IP_3} , is described by

$$Ca_{IP_3} = IP_3 \cdot \frac{G_{IP_3R}}{V}. \quad (31)$$

These reactions are simulated by the use of Gillespie's method and τ -leap method²⁹. The τ -leap method by Cao *et al.* shows good approximation for the first-order reactions like this study³⁰.

We defined the Ca_{res} as the AUC of the time course of Ca^{2+} , given by

$$Ca_{res} = \int_T \{[Ca](t) - C_b\} dt, \quad (32)$$

where C_b denotes the basal concentration of Ca^{2+} , which is 41.6 nM. Note that Koumura *et al.*²² defined Ca_{res} as the logarithmic AUC, which is different from that in this study, however, the results of this study qualitatively show the same results.

The values of the parameters in the simple stochastic model are shown in Supplementary Table 1 and 2. The parameters excluding the follows are the same as the simple deterministic model²².

Mutual information between the PF- and CF-timing and Ca^{2+} increase

We measured the input timing information coded by the Ca^{2+} response by mutual information between the Ca_{res} and PF-CF timing interval $\Delta t = t_{CF} - t_{PF}$, given by

$$I(Ca_{res}; \Delta t) = \int_{\Delta t} p_{in}(\tau) \left(\int_{Ca_{res}} p_c(c|\tau) \log_2 \frac{p_c(c|\tau)}{\int_{\Delta t} p_{in}(\tau) p_c(c|\tau) d\tau} dc \right) d\tau. \quad (33)$$

Here, the $p_{in}(\Delta t)$ follows the uniform distribution. To remove the bias by the bin width of Ca_{res} , the mutual information was calculated by the method introduced by Cheong *et al.*³¹. The mutual information remains the almost constant for the bin width between 10^{-2} and $10^{-3.5} \mu\text{m}^3$. Therefore, we fixed the bin width of Ca_{res} as $10^{-2} [\text{pM} \cdot \text{min}]$ in the analysis and drawing the histogram.

We also measured the information coded by the probability of the large Ca^{2+} increase and by the amplitude of the Ca^{2+} increase, denoted as the mutual information of the probability component and of the amplitude component, respectively. We defined θ as the Ca_{res} representing the local minimum value of the marginal distribution $p_c(Ca_{res})$ (Fig. 1) and s as the logical value whether $Ca_{res} > \theta$ is satisfied or not.

The mutual information coded of the probability component is defined as

$$I_{prob}(Ca_{res}; \Delta t) = \int_{\Delta t} p_{in}(\tau) \left(\int_{Ca_{res}} p_c(c|\tau) \log_2 \frac{p_c(c|\tau)}{p_{-prob}(c|\tau)} dc \right) d\tau, \\ p_{-prob}(Ca_{res}|\Delta t) = \sum_{s \in \{0,1\}} P(s) p_c(Ca_{res}|s, \Delta t), \quad (34)$$

where $p_{-prob}(Ca_{res}|\Delta t)$ denotes the distribution of Ca_{res} without the probability component, which was calculated by marginalizing Δt out of the probability component $p_c(s|\Delta t)$ in $p_c(Ca_{res}|\Delta t)$.

The mutual information coded by the amplitude component is defined as

$$I_{amp}(Ca_{res}; \Delta t) = \int_{\Delta t} p_{in}(\tau) \left(\int_{Ca_{res}} p_c(c|\tau) \log_2 \frac{p_c(c|\tau)}{p_{-amp}(c|\tau)} dc \right) d\tau,$$

$$p_{-amp}(Ca_{res}|\Delta t) = \sum_{s \in \{0,1\}} P(s|\Delta t) p_c(Ca_{res}|s), \quad (35)$$

where $p_{-amp}(Ca_{res}|\Delta t)$ denotes the distribution of Ca_{res} without the amplitude component, which was calculated by marginalizing Δt out of the amplitude component $p_c(Ca_{res}|s, \Delta t)$ in $p_c(Ca_{res}|\Delta t)$. These informations satisfies

$$I(Ca_{res}; \Delta t) = I_{prob}(Ca_{res}; \Delta t) + I_{amp}(Ca_{res}; \Delta t). \quad (36)$$

Mutual information between the amplitude of PF input and Ca^{2+} increase

We also calculated the mutual information between Ca_{res} and Amp_{PF} assuming the input distribution as the Gaussian distribution with μ_s , the average, and STD , the standard deviation, given by

$$I(Ca_{res}; Amp_{PF}) = \int_{Amp_{PF}} p_s(a|\mu_s, STD) \left(\int_{Ca_{res}} p_c(c|a) \log_2 \frac{p_c(c|a)}{\int_{Amp_{PF}} p_s(a|\mu_s, STD) p_c(c|a) da} dc \right) da, \quad (37)$$

where

$$p_s(Amp_{PF}|\mu_s, STD) = \frac{1}{\sqrt{2\pi}STD} \exp \left[-\frac{(Amp_{PF} - \mu_s)^2}{2STD^2} \right]. \quad (38)$$

Note that p_s and p_a have Amp_{PF} as the variable and are assumed as a Gaussian distribution. However, these distributions mean different feature. p_s means the input distribution of the mutual information, and p_a means the distribution of amplitude of PF input under the fluctuation of amplitude of PF input.

Fitted function of the volume-dependency of mutual information

The mutual information per PF input against the volume was fitted by the functions, $a \log_2(b + cV)/V$ and $1/2 \log_2(1 + cV)/V$ (Fig. 6b), by use of the Nonlinear Least Squares method with the Marquadt-Levenberg algorithm. We obtained fitting line, $a \log_2(b + cV)$, with the best fit $a = 0.3924651$, $b = 1.049141$, $c = 1.330285$, and the channel capacity of the Gaussian channel, $1/2 \log_2(1 + cV)$, with the best fit parameter $c = 0.5128671$.

Acknowledgement

We are grateful to Dr. Hidetoshi Urakubo, Dr. Takuya Koumura, Dr. Shinsuke Uda, Dr. Yuichi Sakumura and our laboratory members for their critical reading of this manuscript, and Dr. Tamiki Komatsuzaki for fruitful discussion. This work was supported by The Creation of Fundamental Technologies for Understanding and Control of Biosystem Dynamics, CREST, from the Japan Science and Technology (JST).

Additional information

Author contributions: M.F. and S.K. conceived the project. M.F. constructed the model and performed the stochastic simulation. M.F., K.O. Y.K. M.H. and S.K. analyzed the data. M.F. and K.O. contributed theoretical analysis. M.F. and S.K. wrote the manuscript.

Competing financial interests: The authors declare that they have no conflict of interest.

References

1. Napper, R. M. & Harvey, R. J. Number of parallel fiber synapses on an individual Purkinje cell in the cerebellum of the rat. *J. Comp. Neurol.* **274**, 168–77 (1988).
2. Stuart, G., Spruston, N. & Häusser, M. *Dendrites*. (Oxford University Press, 2007).
doi:10.1093/acprof:oso/9780198566564.001.0001
3. Harris, K. M. & Stevens, J. K. Dendritic spines of rat cerebellar Purkinje cells: serial electron microscopy with reference to their biophysical characteristics. *J. Neurosci.* **8**, 4455–69 (1988).
4. Rapp, M., Segev, I. & Yarom, Y. Physiology, morphology and detailed passive models of guinea-pig cerebellar Purkinje cells. *J. Physiol.* **474**, 101–18 (1994).
5. Takács, J. & Hátori, J. Developmental dynamics of Purkinje cells and dendritic spines in rat cerebellar cortex. *J. Neurosci. Res.* **38**, 515–30 (1994).
6. Antunes, G. & De Schutter, E. A stochastic signaling network mediates the probabilistic induction of cerebellar long-term depression. *J. Neurosci.* **32**, 9288–300 (2012).
7. Anwar, H., Hepburn, I., Nedelescu, H., Chen, W. & De Schutter, E. Stochastic calcium mechanisms cause dendritic calcium spike variability. *J. Neurosci.* **33**, 15848–67 (2013).
8. Barbour, B. Synaptic currents evoked in Purkinje cells by stimulating individual granule cells. *Neuron* **11**, 759–69 (1993).

9. Okubo, Y. *et al.* Imaging extrasynaptic glutamate dynamics in the brain. *Proc. Natl. Acad. Sci. U. S. A.* **107**, 6526–31 (2010).
10. Isope, P. & Barbour, B. Properties of unitary granule cell→Purkinje cell synapses in adult rat cerebellar slices. *J. Neurosci.* **22**, 9668–78 (2002).
11. Ito, M. Neurophysiological aspects of the cerebellar motor control system. *Int. J. Neurol.* **7**, 162–76 (1970).
12. Kawato, M. Internal models for motor control and trajectory planning. *Curr. Opin. Neurobiol.* **9**, 718–27 (1999).
13. Kawato, M., Kuroda, S. & Schweighofer, N. Cerebellar supervised learning revisited: biophysical modeling and degrees-of-freedom control. *Curr. Opin. Neurobiol.* **21**, 791–800 (2011).
14. Miyakawa, H., Lev-Ram, V., Lasser-Ross, N. & Ross, W. N. Calcium transients evoked by climbing fiber and parallel fiber synaptic inputs in guinea pig cerebellar Purkinje neurons. *J. Neurophysiol.* **68**, 1178–89 (1992).
15. Wang, S. S., Denk, W. & Häusser, M. Coincidence detection in single dendritic spines mediated by calcium release. *Nat. Neurosci.* **3**, 1266–73 (2000).
16. Ito, M. The molecular organization of cerebellar long-term depression. *Nat. Rev. Neurosci.* **3**, 896–902 (2002).
17. Mauk, M. D., Garcia, K. S., Medina, J. F. & Steele, P. M. Does cerebellar LTD mediate motor learning? Toward a resolution without a smoking gun. *Neuron* **20**, 359–62 (1998).
18. Steinmetz, J. E. Classical nictitating membrane conditioning in rabbits with varying interstimulus intervals and direct activation of cerebellar mossy fibers as the CS. *Behav. Brain Res.* **38**, 97–108 (1990).
19. Doi, T., Kuroda, S., Michikawa, T. & Kawato, M. Inositol 1,4,5-trisphosphate-dependent Ca²⁺ threshold dynamics detect spike timing in cerebellar Purkinje cells. *J. Neurosci.* **25**, 950–61 (2005).
20. Honda, M., Urakubo, H., Koumura, T. & Kuroda, S. A common framework of signal processing in the induction of cerebellar LTD and cortical STDP. *Neural Netw.* **43**, 114–24 (2013).
21. Honda, M., Urakubo, H., Tanaka, K. & Kuroda, S. Analysis of development of direction selectivity in retinotectum by a neural circuit model with spike timing-dependent plasticity. *J. Neurosci.* **31**, 1516–27 (2011).
22. Koumura, T., Urakubo, H., Ohashi, K., Fujii, M. & Kuroda, S. Stochasticity in Ca²⁺ increase in spines enables robust and sensitive information coding. *PLoS One* **9**, e99040 (2014).
23. Rancz, E. A. & Häusser, M. Dendritic calcium spikes are tunable triggers of cannabinoid release and short-term synaptic plasticity in cerebellar Purkinje neurons. *J. Neurosci.* **26**, 5428–37 (2006).
24. Jin Wang & Peter Wolynes. Intermittency of single molecule reaction dynamics in fluctuating environments. *Phys. Rev. Lett.* **74**, 4317–4320 (1995).

25. McDonnell, M. D. & Ward, L. M. The benefits of noise in neural systems: bridging theory and experiment. *Nat. Rev. Neurosci.* **12**, 415–426 (2011).
26. Garaschuk, O., Schneggenburger, R., Schirra, C., Tempia, F. & Konnerth, A. Fractional Ca²⁺ currents through somatic and dendritic glutamate receptor channels of rat hippocampal CA1 pyramidal neurones. *J. Physiol.* **491**, 757–772 (1996).
27. Kubota, S. & Kitajima, T. A model for synaptic development regulated by NMDA receptor subunit expression. *J. Comput. Neurosci.* **24**, 1–20 (2008).
28. Lester, R. A. J. & Jahr, C. E. NMDA channel behavior depends on agonist affinity. *J. Neurosci.* **12**, 635–643 (1992).
29. Cao, Y., Gillespie, D. T. & Petzold, L. R. Efficient step size selection for the tau-leaping simulation method. *J. Chem. Phys.* **124**, 044109 (2006).
30. Gillespie, D. T., Hellander, A. & Petzold, L. R. Perspective: Stochastic algorithms for chemical kinetics. *J. Chem. Phys.* **138**, 170901 (2013).
31. Cheong, R., Rhee, A., Wang, C. J., Nemenman, I. & Levchenko, A. Information Transduction Capacity of Noisy Biochemical Signaling Networks. *Science (80-.)*. **334**, 354–358 (2011).

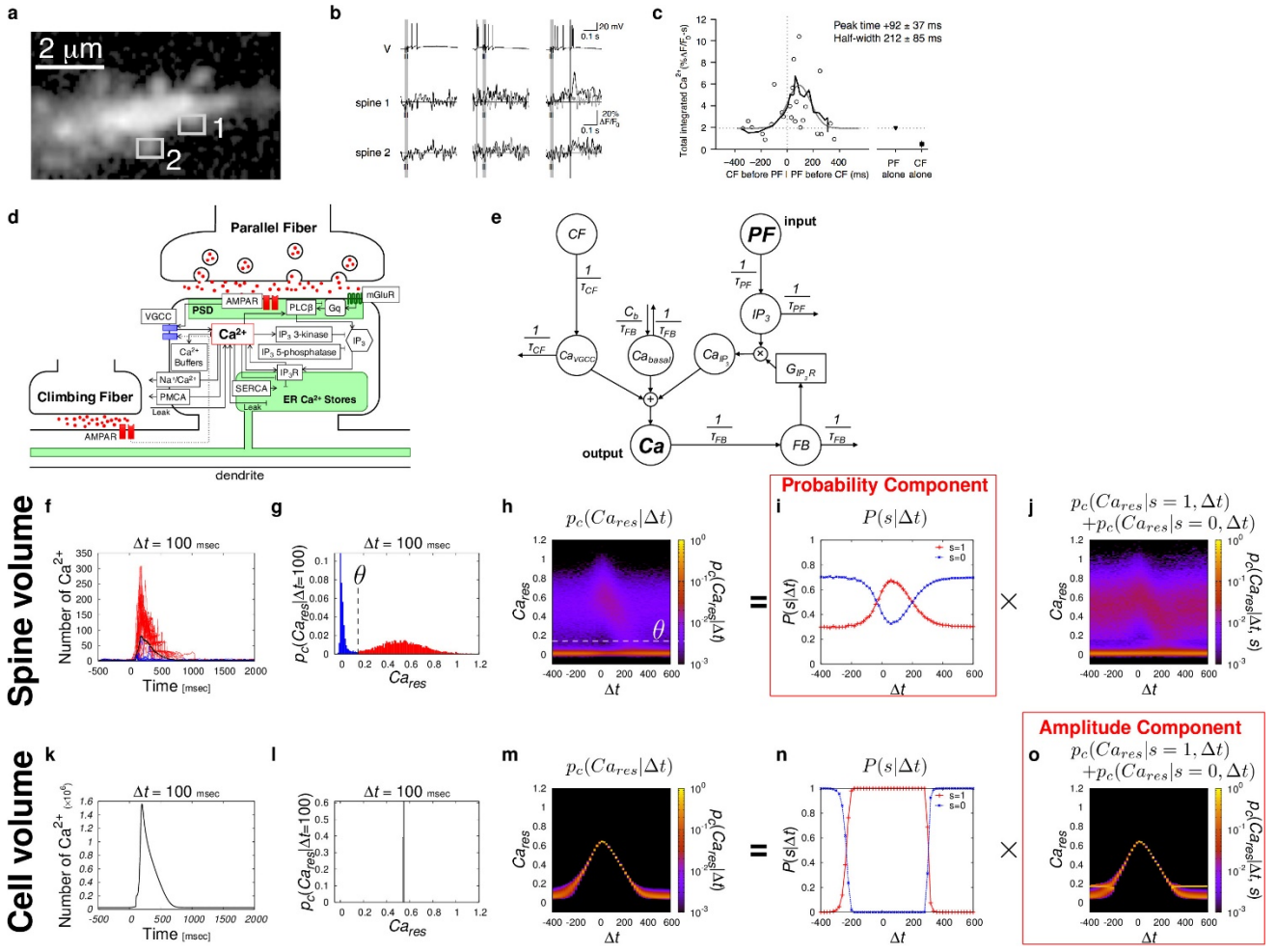


Figure 1 | Information transfer of PF- and CF-timing by probability of Ca^{2+} increase in the simple stochastic model.

(a-c) Experimental results of Ca^{2+} increase by PF and CF inputs at the spine in the cerebellar Purkinje cell¹⁵. (a) Spines of the cerebellar Purkinje cell. (b) Ca^{2+} response in the indicated spines in (a). V indicates membrane potential and $\Delta\text{F}/\text{F}_0$ indicates the normalized changes of the fluorescence probe of Ca^{2+} . The left, middle, and right panels show the time courses with only the PF input (shaded vertical line), with the CF input (black vertical line) before 60 msec before the PF input, and with the PF input 60 msec before the CF input, respectively. (c) Total integrated Ca^{2+} with PF and CF inputs with various timing. The gray line indicates the best fits of the raw data points to Gaussian functions. The black line indicates the box-smoothed average over three points. (d) Schematic representation of Ca^{2+} increase by PF and CF inputs in the detailed stochastic model²². (e) The block diagram of the simple stochastic model in this study (see Methods). After Fig. 3, we set $CF = 0$, and used only PF as the input. Ca^{2+} increase in the spine volume ($10^{-1} \mu\text{m}^3$) (f–j) in the cell volume ($10^3 \mu\text{m}^3$) (k–o) in the simple stochastic model. (f, k), Ca^{2+} increase with $\Delta t = 100$ msec. Δt indicates the timing interval between PF and CF inputs, which is set the timing of PF input as 0, and Δt with the PF input before CF input is positive and *vice versa*. In (f), the large Ca^{2+} increase (red) and small Ca^{2+} increase (blue) divided by θ in (g). (g, l), the probability

density distribution of Ca_{res} . Ca_{res} denotes the area under the curve of the time course of Ca^{2+} shown in (f and k). In (g), the threshold θ is defined as the local minimum of the marginal distribution for Δt , given by $p_c(Ca_{res}) = \int_{\Delta t} p_c(Ca_{res}|\tau)p_{in}(\tau) d\tau$ (see Supplementary Fig. 1). (h, m), the probability density distribution of Ca_{res} in the spine volume (h) and cell volume (m). (i, n), the probability component of the distribution of Ca_{res} that exceeds the threshold θ in the spine volume ($s = 1$) (see Methods). Since the distribution of Ca_{res} in the cell volume is unimodal distribution, for convenience, we set $\theta = 0.157$ in the cell volume, the same as that in the spine volume. (j, o), the amplitude component of the distribution of Ca_{res} (see Methods)

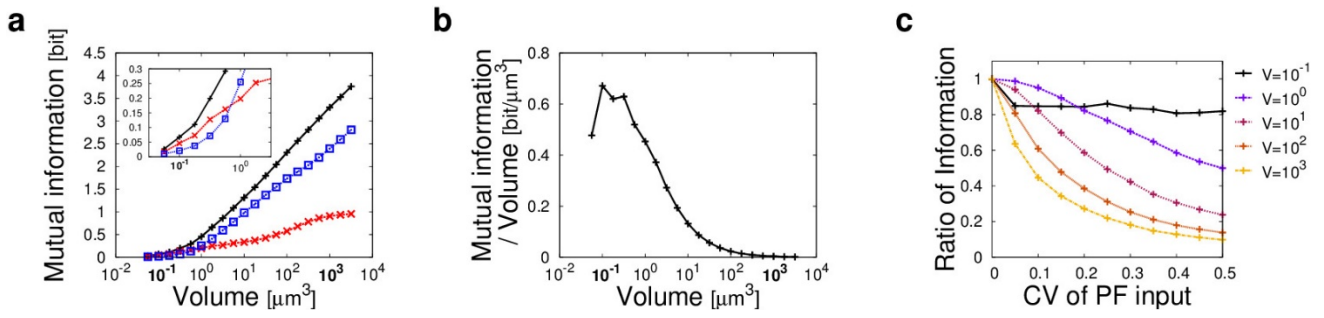


Figure 2 | The efficient and robust features in the simple stochastic model. (a) The volume-dependency of the mutual information between the PF- and CF-timing and Ca_{res} . The black, red, blue lines indicate the mutual information of the total distribution of Ca_{res} , of the probability component and of the amplitude component, respectively. (b) The volume-dependency of the mutual information per volume. (c) CV of amplitude of PF input-dependency of the mutual information. The ratio of information was obtained by setting mutual information with CV = 0 for each volume at 1.

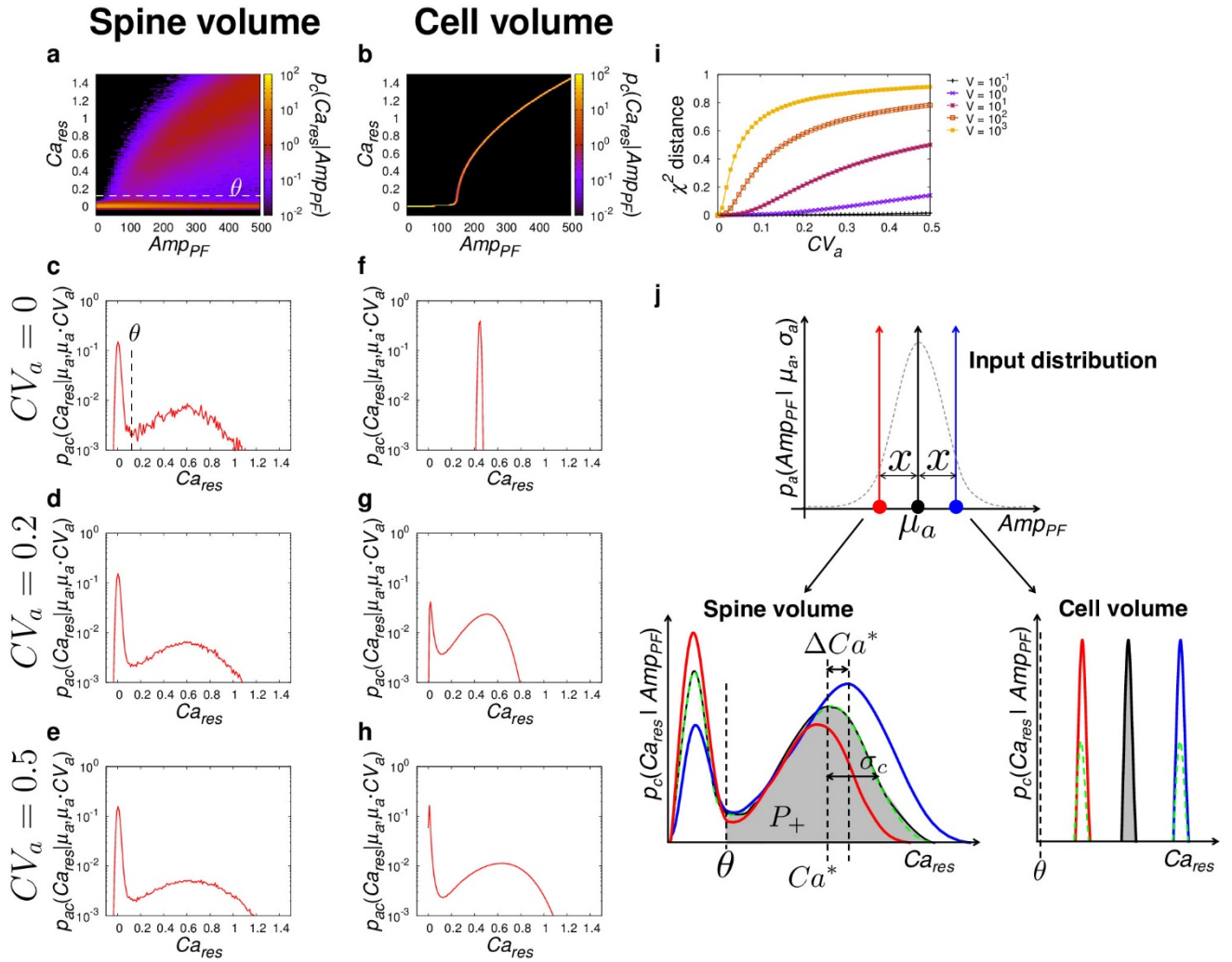


Figure 3 | Unchanging of distributions of Ca_{res} against fluctuation of PF input gives robustness in the spine volume.

The Amp_{PF} -dependency of $p_c(Ca_{res}|Amp_{PF})$, the distributions of Ca_{res} , in the spine volume (a) and in the cell volume (b). (c–h) The distributions of Ca_{res} against the PF input fluctuation with the indicated CV_a with $\mu_a = 180$ in the spine volume (c–e) and in the cell volume (f–h), respectively. θ indicates the threshold dividing the distribution into the ranges with large Ca_{res} and with small Ca_{res} (see Supplementary Fig. 1). (i) The CV_a -dependency of χ^2 distance of distributions between $p_{ac}(Ca_{res}|\mu_a, \mu_a \cdot CV_a)$ and $p_{ac}(Ca_{res}|\mu_a, 0)$ with $\mu_a = 180$. (j) The input distribution of Amp_{PF} is given by the Gaussian distribution $\mathcal{N}(\mu_a, \sigma_a^2)$. The distribution of Ca_{res} with $Amp_{PF} = \mu_a$ (black), $Amp_{PF} = \mu_a + x$ (blue), and $Amp_{PF} = \mu_a - x$ (red) in the spine volume (left) and the cell volume (right). The averaged distribution of the distributions with $Amp_{PF} = \mu_a + x$ and with $Amp_{PF} = \mu_a - x$ (green).

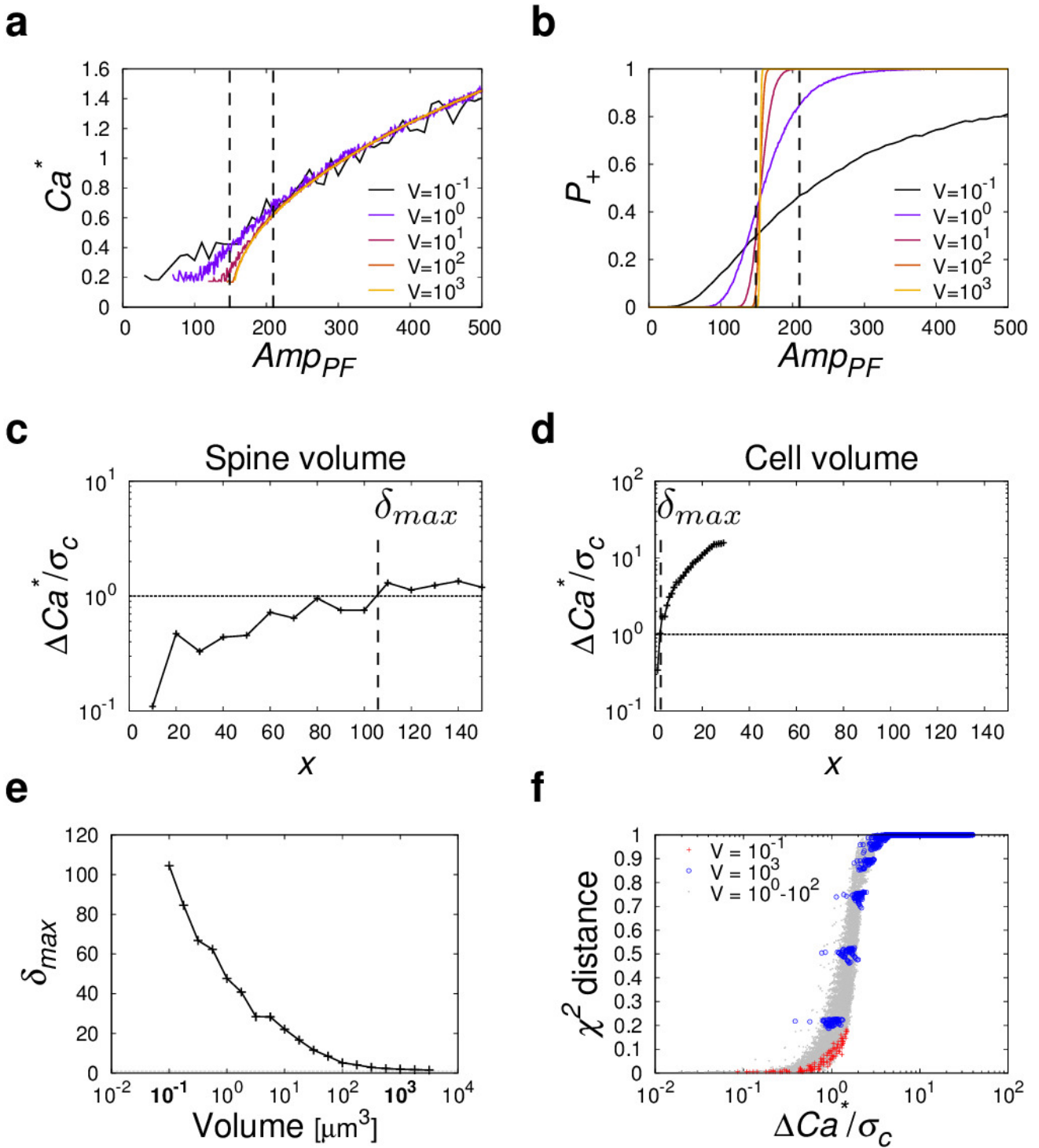


Figure 4 | The ratio between extrinsic and intrinsic noise, $\Delta Ca^*/\sigma_c$, determines the range of the robustness. (a) The Amp_{PF} -dependency of the Ca_{res} realizing the peak of distribution of Ca_{res} for $Ca_{res} > \theta$, Ca^* . (b) The Amp_{PF} -dependency of the probability of $Ca_{res} > \theta$, P_+ . (c, d) $Amp'_{PF} = x$, the relative amplitude of PF input,-dependency of $\Delta Ca^*/\sigma_c$ with $\mu_a = 180$ in the spine volume (c) and the cell volume (d). The robustness index δ_{max} is defined as x giving $\Delta Ca^*/\sigma_c = 1$ (e) The volume-dependency of δ_{max} for $\mu_a = 180$. (f) The relationship between $\Delta Ca^*/\sigma_c$ and the χ^2 distance

between the averaged distribution of the distributions of Ca_{res} with $Amp'_{PF} = \pm x$ and the distribution of Ca_{res} with $Amp'_{PF} = 0$. The red points, blue points, and gray dots indicate the value obtained in the spine volume, the cell volume and the intermediate volumes, respectively.

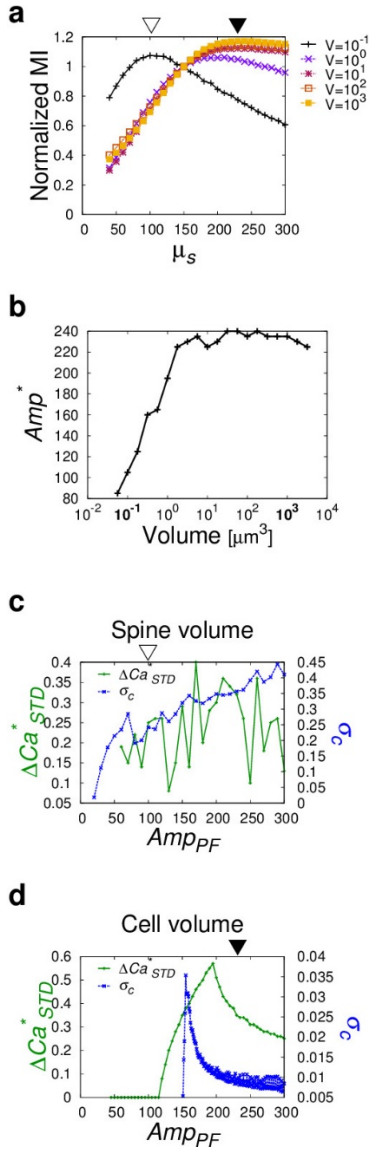


Figure 5 | The mechanism of the sensitivity. (a) μ_s , the average of input distribution of Amp_{PF} , -dependency of the mutual information. The mutual information is normalized by the value of that with $\mu_s = 150$. The brighter color indicates the larger volume. The white and black triangles denote Amp^* , the amplitude of the PF input realizing the maximum of the mutual information, in the spine volume and in the cell volume, respectively. $Amp^* = 100$ in the spine volume, and $Amp^* = 235$ in the cell volume. The input distribution of Amp_{PF} is utilized as the Gaussian distribution with the standard deviation, STD , 40. (b) The volume-dependency of the amplitude of the PF input realizing the maximum of the mutual information, Amp^* . (c, d) The Amp_{PF} -dependencies of ΔCa_{STD}^* , the dynamic range of the distribution of Ca_{res} for $Ca_{res} > \theta$ (green), and σ_c , the standard deviation of the distribution of Ca_{res} (blue). $STD = 40$ was used. The white and black triangles denote Amp^* in the spine volume and in the cell volume, respectively.

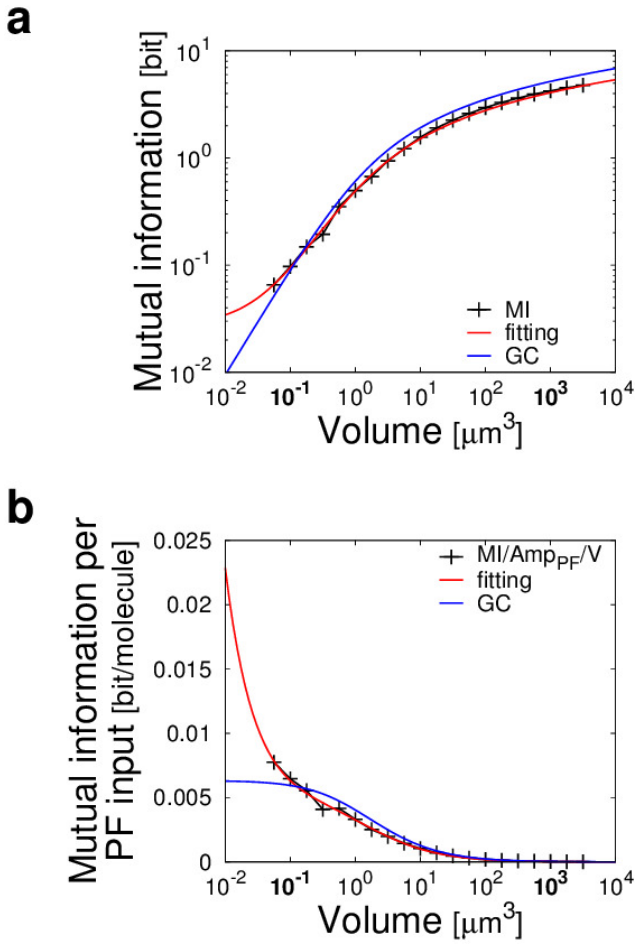


Figure 6 | The mechanism of the efficiency. (a) The volume-dependency of the mutual information between Amp_{PF} and Ca_{res} . (b) The volume-dependency of the mutual information per PF input, *i.e.* the efficiency. The total mutual information, black; the fitted curve of the total mutual information by $a \log_2(b + cV)$ with $a = 0.3924651$, $b = 1.049141$, $c = 1.330285$, red; the channel capacity of the Gaussian channel, $1/2 \log_2(1 + cV)$ with $c = 0.5128671$, blue (see Methods). We assume the input distribution of Amp_{PF} as the Gaussian distribution with $\mu_s = 150$, the average of amplitude of the distribution of the PF input, and $STD = 40$, the standard deviation of the distribution of the PF input.

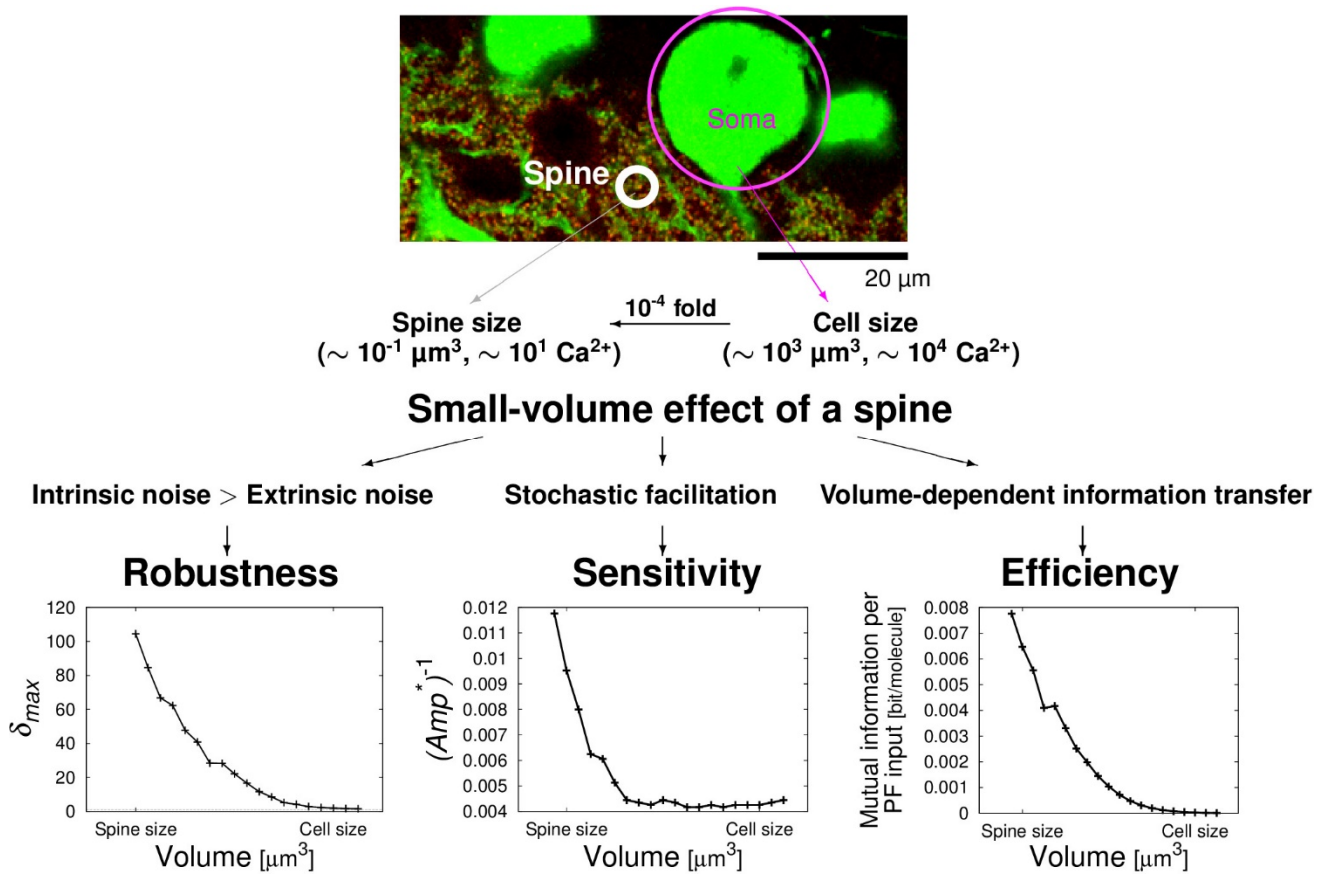
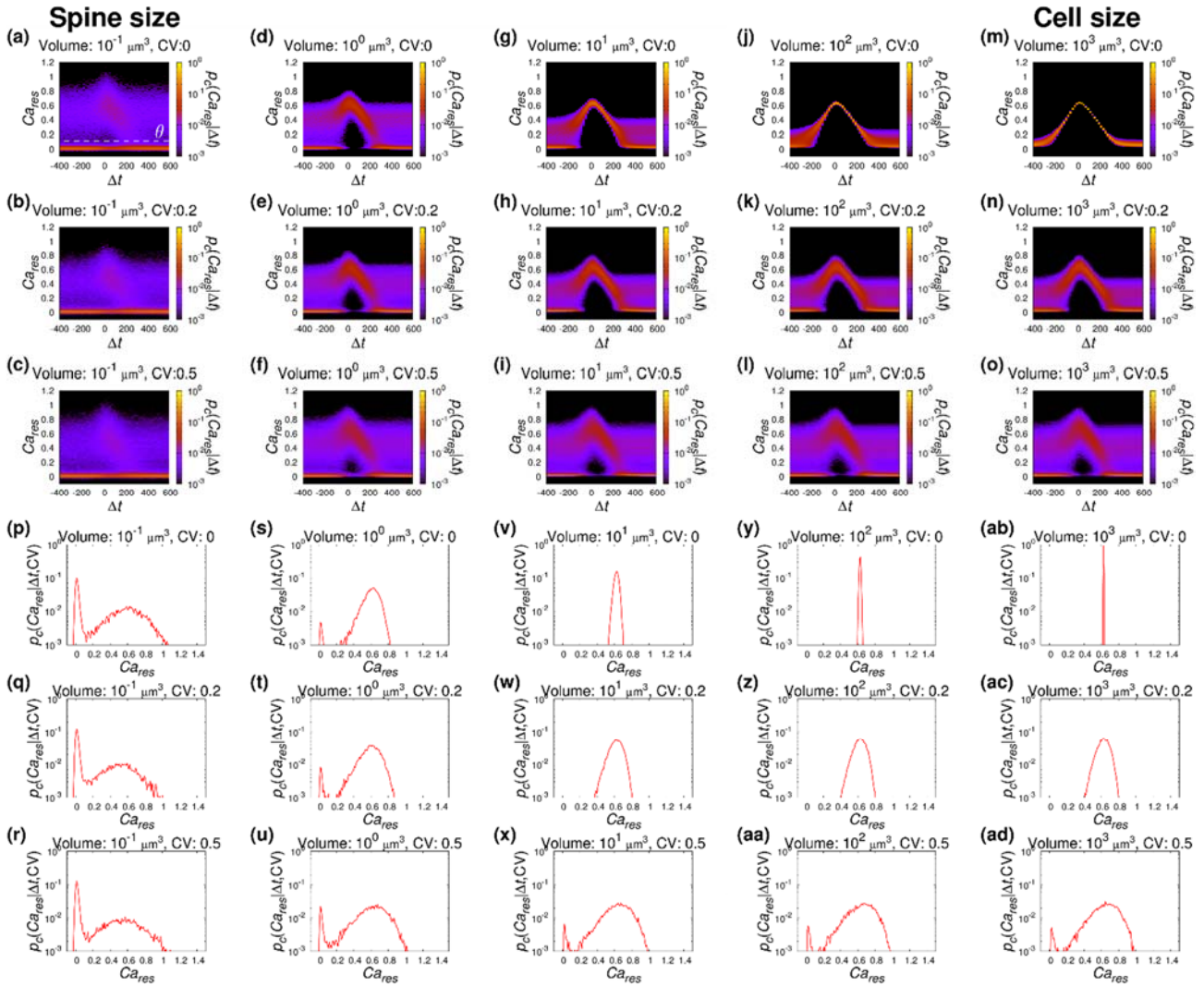
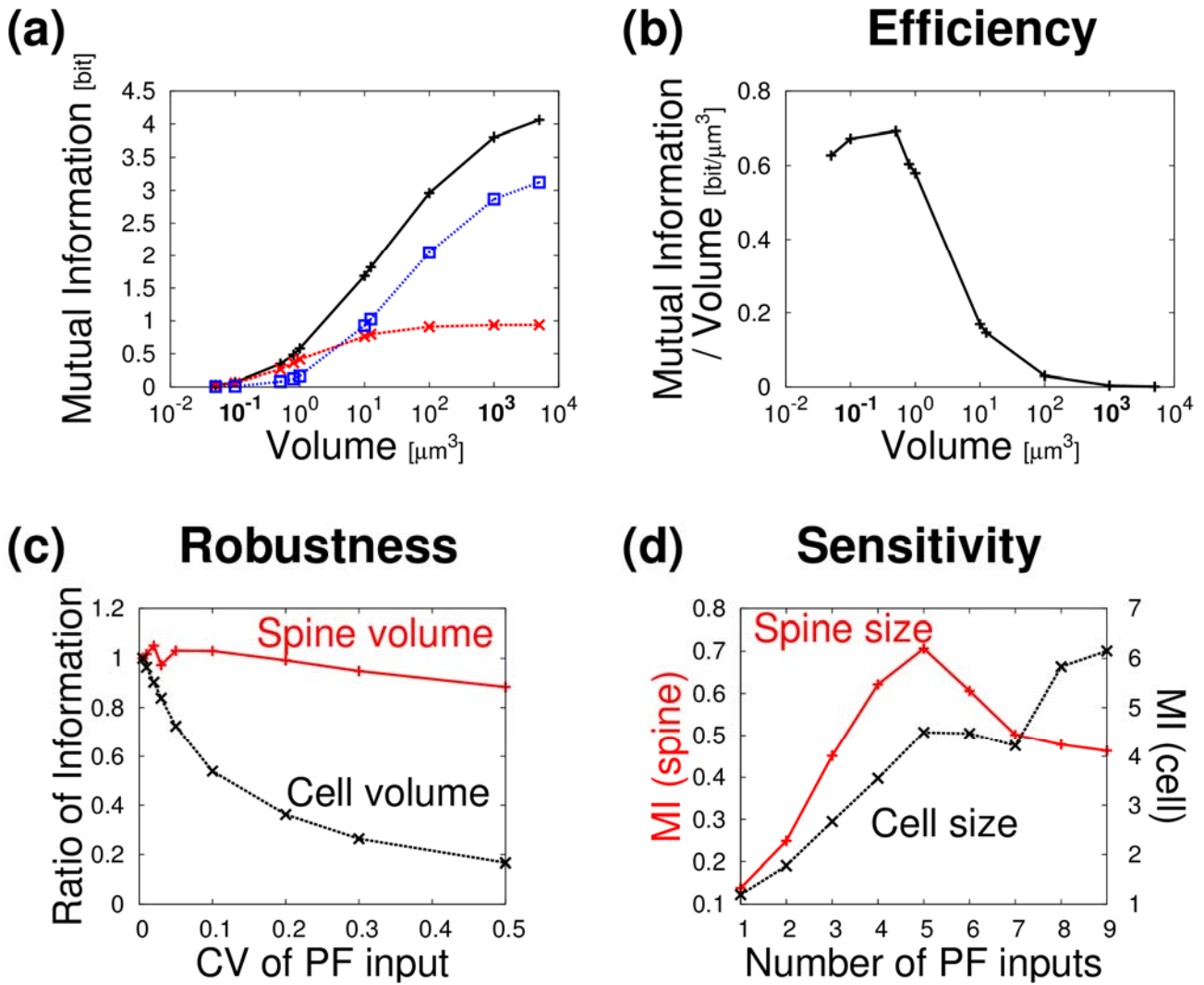


Figure 7 | Summarizing figure. The small-volume effect enables the spine robust, sensitive and efficient information transfer. Robustness appears when intrinsic noise is larger than extrinsic noise. Sensitivity appears because of the stochastic facilitation. Note that, as index for the sensitivity in this figure, the inverse of Amp^* (Fig. 5b) is used. Efficiency appears because of the nature of volume-dependency of information transfer.

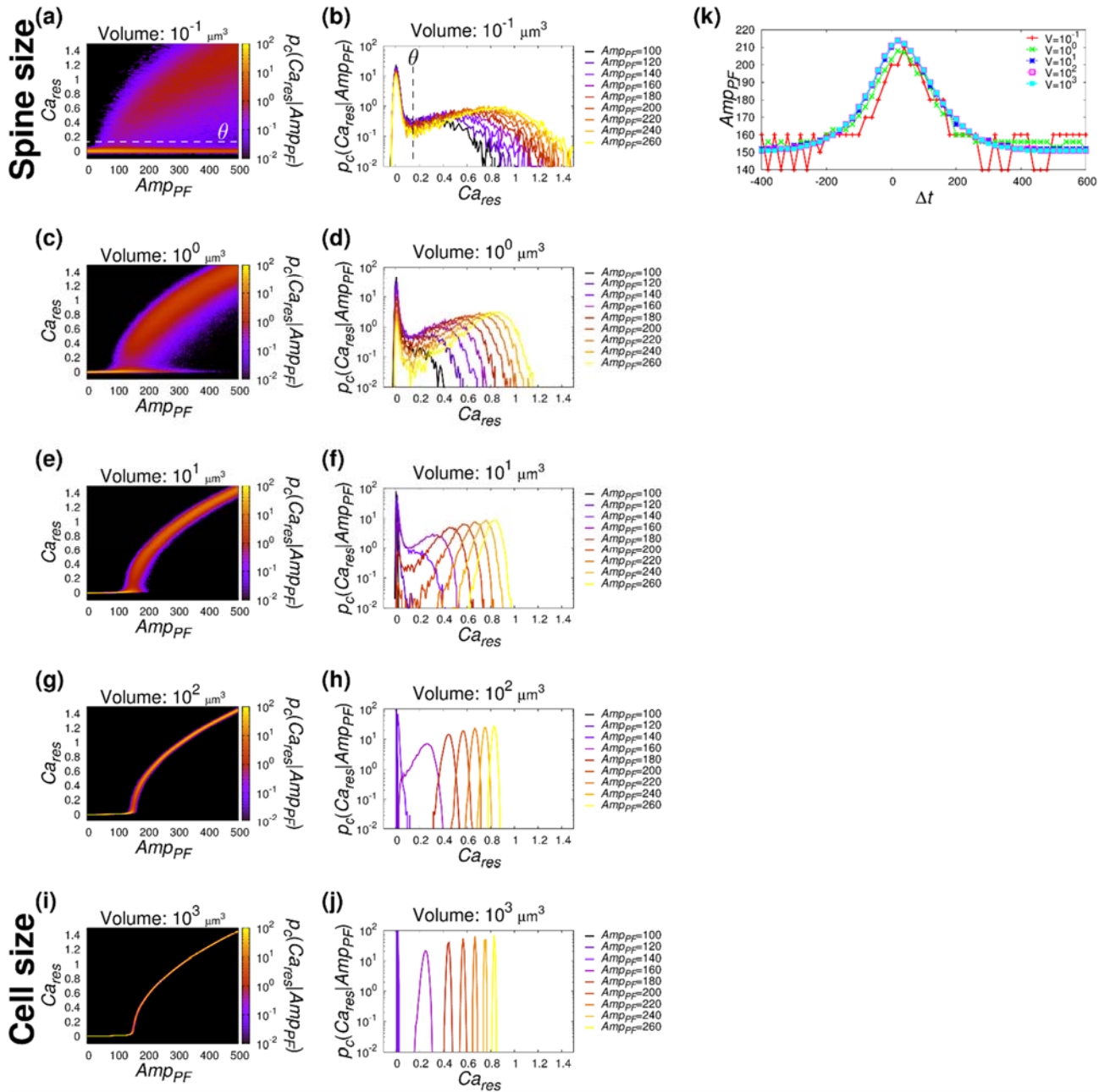
Supplementary Information



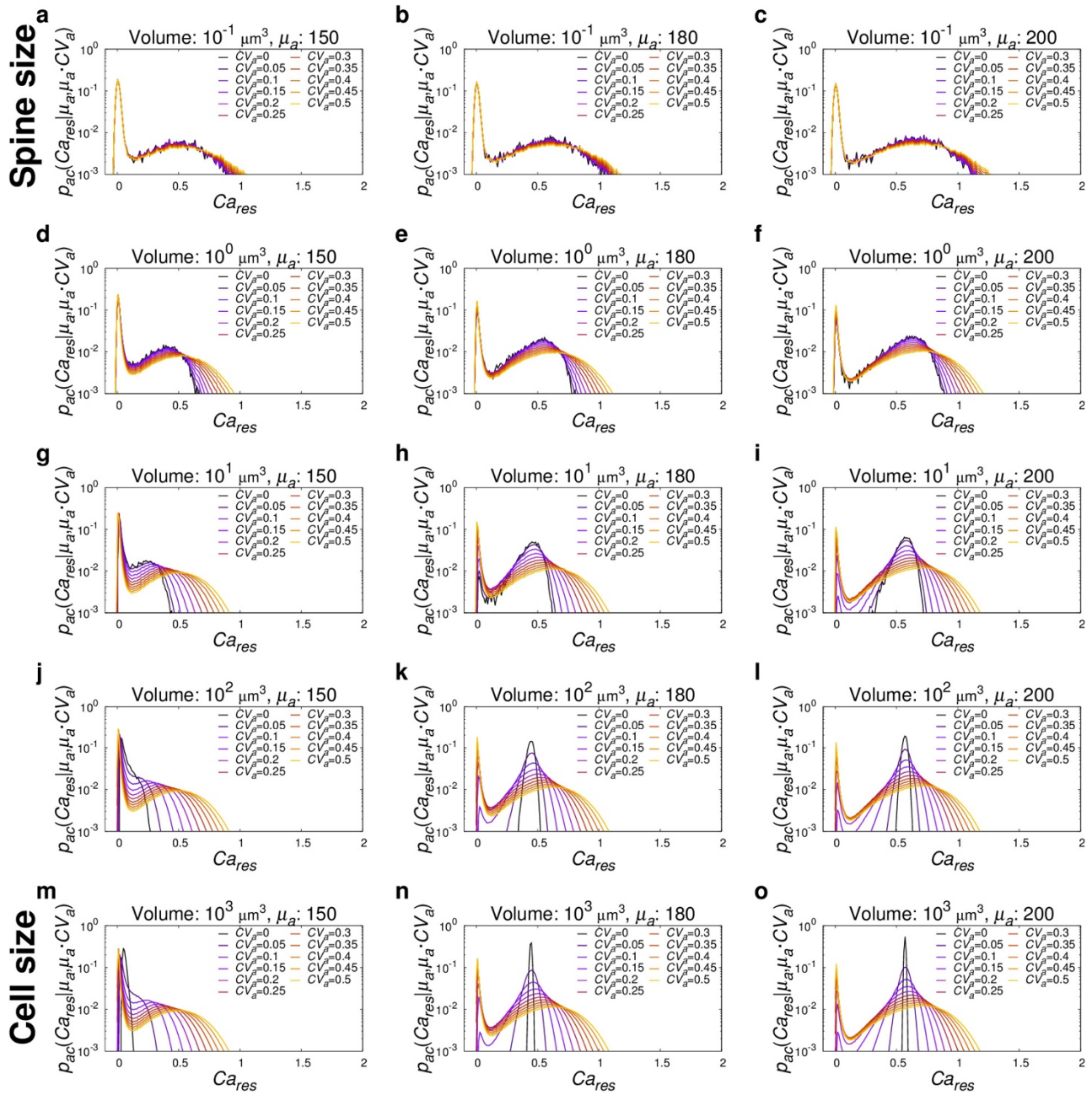
Supplementary Figure 1 | (a–o) The Δt -dependency of the distribution of Ca_{res} . The volume and the CV of amplitude of PF input are indicated. In the spine volume, the distribution of Ca_{res} is divided into two distributions by threshold $\theta = 0.157$ defined as the local minimum of the marginal distribution of Ca_{res} for Δt *s.t.* $p_c(Ca_{res}) = \int_{\Delta t} p_{in}(\tau) p_c(Ca_{res}|\tau) d\tau$. (p–ad) The cross sections of (a–o) with $\Delta t = 0$. This distribution of Ca_{res} in the spine volume remained the same regardless of the CV_a value, whereas, that in the cell volume largely varied.



Supplementary Figure 2 | The efficient, robust and sensitive features of Ca^{2+} increase in the previous study using the detailed stochastic model²². (a) The volume-dependency of the mutual information between the PF- and CF-timing, Δt , and Ca^{2+} response, Ca_{res} . The total mutual information, black; that of the probability component, red; that of the amplitude component, blue. (b) The volume-dependency of the mutual information per volume. (c) The CV of amplitude of PF input-dependency of the mutual information. (d) The number of PF inputs-dependency of the mutual information. In the detailed stochastic model, we denote that the spine volume is $10^{-1} \mu\text{m}^3$ and the cell volume is $5 \times 10^3 \mu\text{m}^3$ ²².

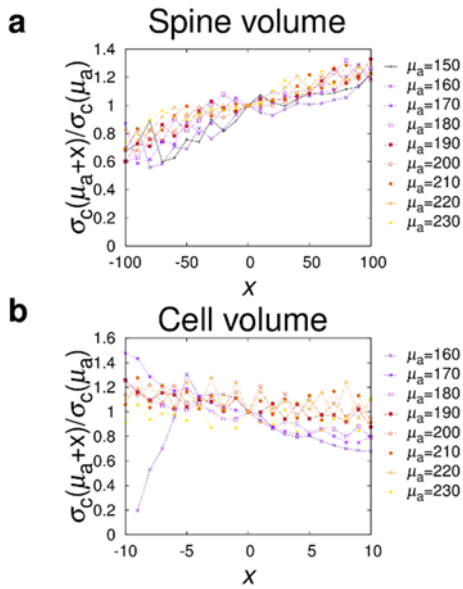


Supplementary Figure 3 | The Amp_{PF} -dependency of the distribution of Ca_{res} in the indicated volumes. (a, c, e, g, i) The distribution of Ca_{res} . (b, d, f, h, j) The cross section of distribution of Ca_{res} at the indicated Amp_{PF} . $\theta(=0.157)$ indicates the threshold dividing the distribution into the ranges with large Ca_{res} and with small Ca_{res} (see Supplementary Fig. 1). (k) The Amp_{PF} that gives $p_c(Ca_{res}|Amp_{PF})$, the distribution of Ca_{res} with PF input alone, closest to $p_c(Ca_{res}|\Delta t)$, the distribution of Ca_{res} with PF and CF inputs with various Δt .

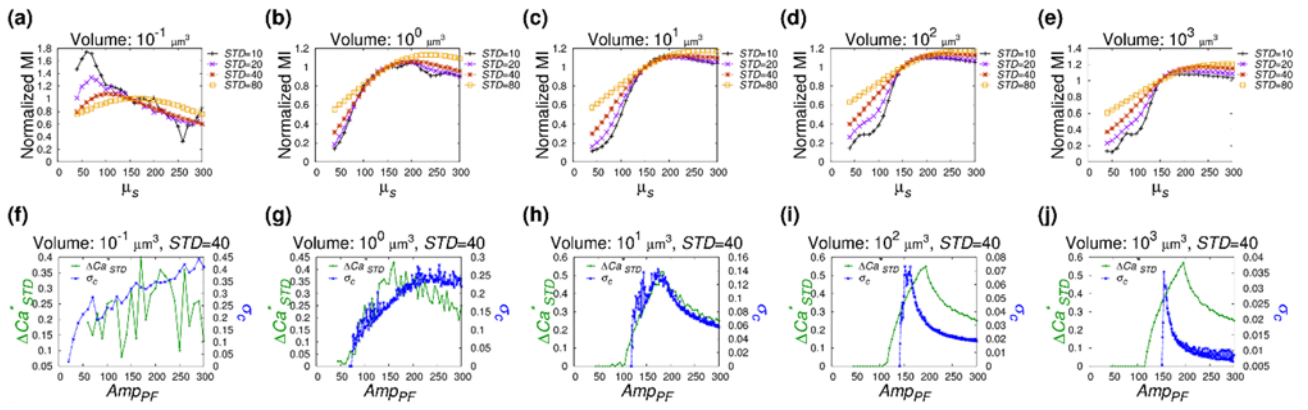


Supplementary Figure 4 | The distributions of Ca_{res} against CV_a with the indicated volumes and the average of Amp_{PF} ,

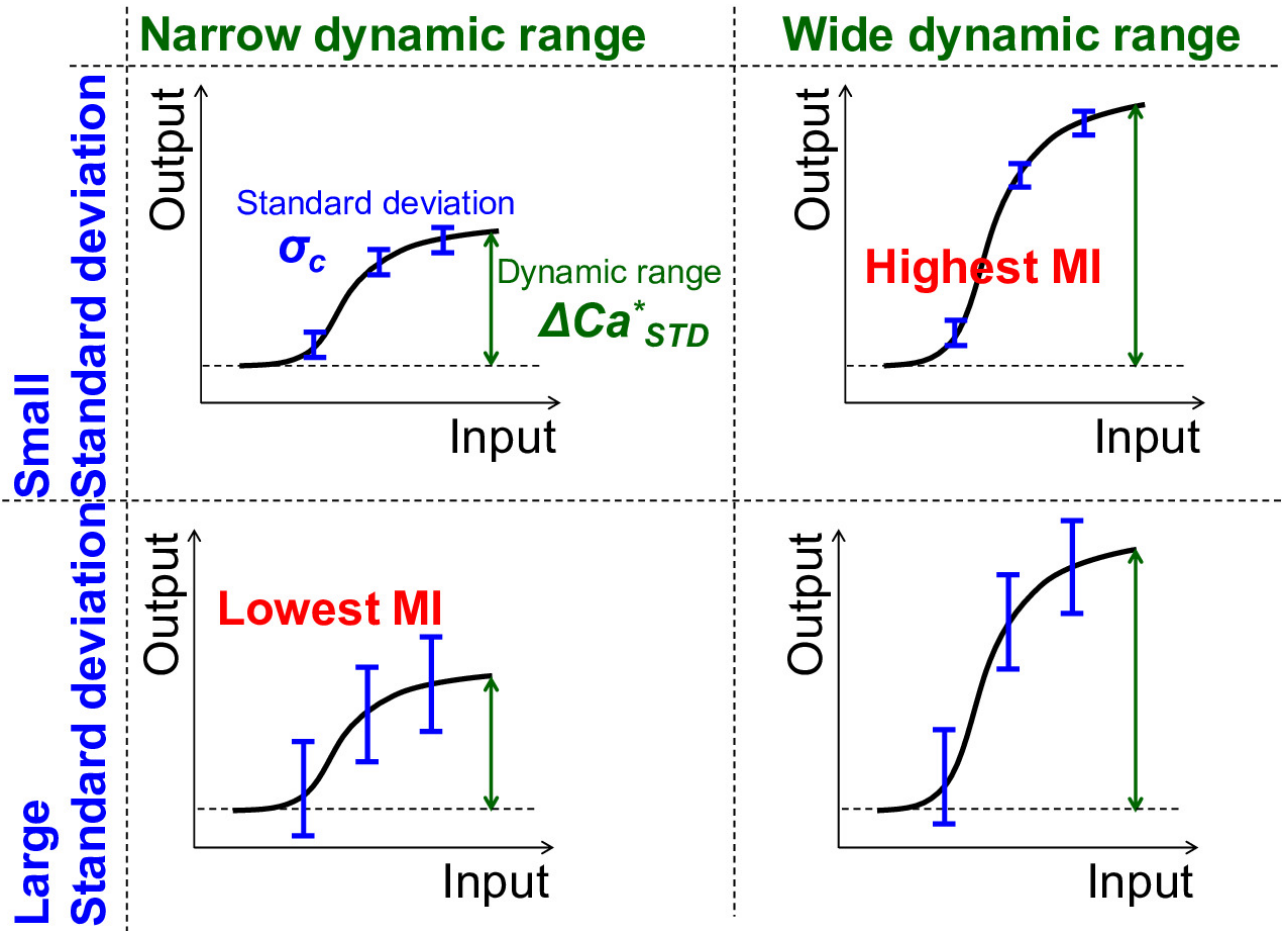
μ_a .



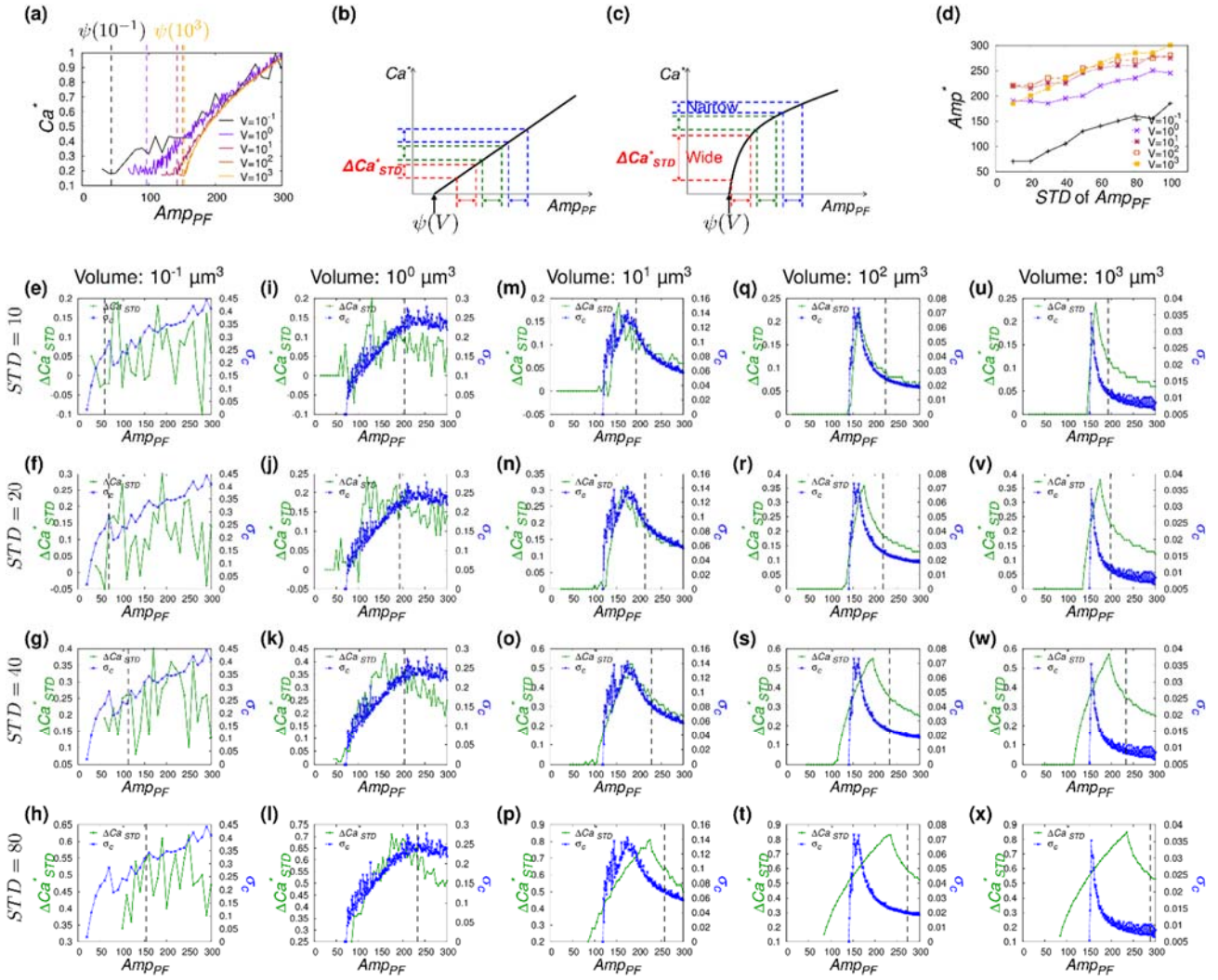
Supplementary Figure 5 | $\sigma_c(\mu_a + x)$ can be regarded as $\sigma_c(\mu_a)$ up to the upper bound of the range of x satisfying the equation (4). (a) the spine volume. (b) the cell volume. $\sigma_c(\mu_a + x) / \sigma_c(\mu_a)$ were almost within the range between 0.8 and 1.2, assuming that $\sigma_c(\mu_a + x)$ is approximated by $\sigma_c(\mu_a)$. The upper bound of the range of x satisfying the equation (4) in the spine and cell volumes are determined by δ_{\max} (see Fig. 4c, d).



Supplementary Figure 6 | The mechanism of the sensitivity. (a–e) μ_s , the average of input distribution of Amp_{PF} , -dependency of the mutual information normalized by the value of that with $\text{Amp}_{PF} = 150$. (f–j) The Amp_{PF} -dependencies of the dynamic range of the distribution of Ca_{res} for $\text{Ca}_{res} > \theta$. The volume is indicated.



Supplementary Figure 7 | The mutual information depends on both ΔCa^*_{STD} , the dynamic range, and σ_c , the standard deviation of the distribution of the output. In general, if the input distribution is the same, the wider ΔCa^*_{STD} , the dynamic range of the output, gives the higher mutual information when σ_c , the standard deviation of the output, is the same (compare the left and right panels). The smaller σ_c gives the higher mutual information when the ΔCa^*_{STD} is the same (compare the top and bottom panels).



Supplementary Figure 8 | ΔCa^*_{STD} , the dynamic range, and σ_c , the standard deviation of the distribution of the output.

(a) The Amp_{PF} -dependency of Ca^* , Ca_{res} realizing the peak of the distribution of Ca_{res} for $Ca_{res} > \theta$. We defined $\psi(V)$ for each volume as the Amp_{PF} where the Ca^* begins to increase. In the spine volume, $\psi(10^{-1})$ was around 50, whereas, $\psi(10^3)$ was around 150 in the cell volume. (b, c) The schematic representation of the relationship between Amp_{PF} and Ca^* in the spine volume (b) and in the cell volume (c). (d) The STD of Amp_{PF} -dependency of Amp_{PF} giving the maximum of the mutual information, Amp^* . (e–x) The Amp_{PF} -dependencies of ΔCa^*_{STD} , the dynamic range of the distribution of Ca_{res} for $Ca_{res} > \theta$, (green) and σ_c , the standard deviation of the distribution of Ca_{res} (blue). The volume and STD are indicated.

Supplementary Table 1 | Parameters of the simple stochastic model in this study

Parameters	Values
τ_{PF} [msec]	120
τ_{CF} [msec]	10
τ_{FB} [msec]	80
$Amp_{G_{IP_3R}}$	1291.6667
k [$1/\mu\text{m}^3$]	626.3027
K [$1/\mu\text{m}^3$]	626.3027
n_{IP_3R}	2.7
C_b [$1/\mu\text{m}^3$]	27.70185
V [μm^3]	10^{-1} – 10^3

Supplementary Table 2 | Parameters which are different between the cases with various PF- and CF-timing and with single PF input alone. Note that the simple deterministic model showed the same results as that of the detailed deterministic model; however, by the reduction of the model, the PF and CF inputs were non-dimensional values. By the loss of the dimension of the number of molecules, we could not perform the stochastic simulation as it is. Therefore, we re-determined the numbers of PF and CF inputs as follows. For the PF input, the number of PF input becomes smaller than 1 in the spine volume ($0.1 \mu\text{m}^3$), but the number of PF input needs to be the positive integer. We increased the PF input to 6-fold from the simple deterministic model so that the amount of IP_3 , the mediator of PF input, is the same as that in the detailed stochastic model, resulting in the amplitude of a PF input in the spine volume as 3 ($Amp_{PF} \times V = 30.11 \times 0.1 = 3.011 \approx 3$). We reduced the reaction rate constant of the Ca^{2+} release by the binding IP_3 and IP_3R to one sixth to compensate the Ca_{IP_3} . For the CF input, the CF input increased to 6-fold so that the number of Ca^{2+} through the CF input in the simple stochastic model becomes the same amount as that in the detailed stochastic model.

Parameters	Values	
	PF and CF input (Figs. 1, 2)	PF input alone (Figs. 3, 4, 5, 6)
Amp_{CF} [$1/\mu\text{m}^3$]	361.328	None
Amp_{PF} [$1/\mu\text{m}^3$]	30.11×5 times	variable $\times 1$ time
t_{CF} [msec]	variable	None
t_{PF} [msec]	{0, 10, 20, 30, 40}	0
CV of PF input	variable	0 (in simulation)

Supplementary Note 1 | Proof. The distribution of Ca_{res} changes with the fluctuation of Amp_{PF} when the equation (5) in the main text is satisfied.

There does not exist the distribution of Ca_{res} with the fluctuation of Amp_{PF} , $p_{ac}(Ca_{res}|\mu_a, \sigma_a)$, which does not change against the fluctuation of Amp_{PF} under the conditions where the equation (5) in the main text is satisfied.

When the distribution of Ca_{res} with $Amp_{PF} = \mu_a$, $p_c(Ca_{res}|\mu_a)$, is not the same as the averaged distribution of Ca_{res} between with $Amp_{PF} = \mu_a + (a - \mu_a) = a$ and with $Amp_{PF} = \mu_a - (a - \mu_a) = 2\mu_a - a$, $1/2[p_c(Ca_{res}|a) + p_c(Ca_{res}|2\mu_a - a)]$, *i.e.*

$$p_c(Ca_{res}|\mu_a) \neq \frac{1}{2}[p_c(Ca_{res}|a) + p_c(Ca_{res}|2\mu_a - a)]. \quad (1)$$

By the reductio ad absurdum, we demonstrate that $CV_a^* = \sigma_a^*/\mu_a$ of Amp_{PF} satisfying the following equation for $0 < \sigma_a < \sigma_a^*$ corresponding to $0 < CV_a < CV_a^*$ does not exist.

$$\begin{aligned} p_c(Ca_{res}|\mu_a) &\simeq p_{ac}(Ca|\mu_a, \sigma_a) = \int_{\mu_a}^{\infty} \mathcal{N}(a|\mu_a, \sigma_a^2)[p_c(Ca_{res}|a) + p_c(Ca_{res}|2\mu_a - a)] da \\ \Leftrightarrow \int_{\mu_a}^{\infty} \{ &\mathcal{N}(a|\mu_a, \sigma_a^2)[p_c(Ca_{res}|a) + p_c(Ca_{res}|2\mu_a - a)] - 2p_c(Ca_{res}|\mu_a) \} da \simeq 0 \\ \int_{\mu_a}^{\infty} \mathcal{N}(a|\mu_a, \sigma_a^2) &[p_c(Ca_{res}|a) + p_c(Ca_{res}|2\mu_a - a) - 2p_c(Ca_{res}|\mu_a)] da \simeq 0. \end{aligned} \quad (2)$$

This equation means that the distribution of Ca_{res} does not change against the fluctuation of Amp_{PF} . For simplicity, $f(a)$ is defined as

$$f(a) \equiv p_c(Ca_{res}|a) + p_c(Ca_{res}|2\mu_a - a) - 2p_c(Ca_{res}|\mu_a). \quad (3)$$

The equation (2) becomes

$$\begin{aligned} \int_{\mu_a}^{\infty} \mathcal{N}(a|\mu_a, \sigma_a^2) f(a) da &\simeq 0 \\ a \geq \mu_a, f(\mu_a) = 0, f(a) &\neq 0, f(a): \text{Continuous.} \end{aligned} \quad (4)$$

Note that from the equation (1), $f(a) \neq 0$. Here, $g(\sigma_a)$ is defined as

$$g(\sigma_a) = \int_{\mu_a}^{\infty} \mathcal{N}(a|\mu_a, \sigma_a^2) f(a) da, \quad (5)$$

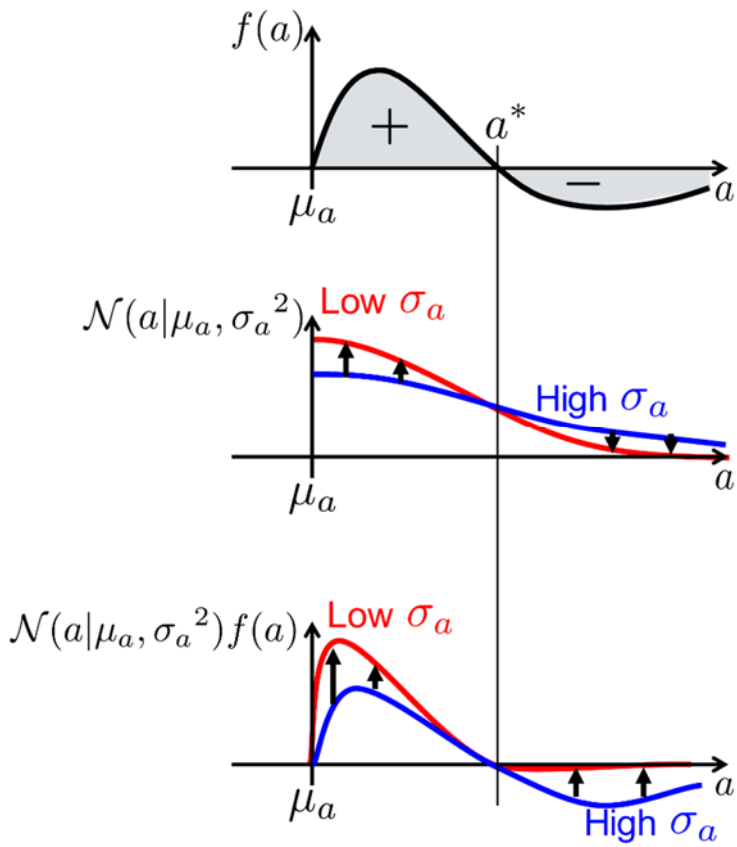
and it is assumed that there exists σ_a satisfying $g(\sigma_a) \equiv 0$ for $0 \leq \sigma_a \leq \sigma_a^*$. From $f(a) \neq 0$ and $f(a)$ is the continuous function, there exists a^* satisfying $f(a) \leq 0$ and $f(a^*) = 0$ for $0 < a < a^*$ (Supplementary Fig. 9, upper panel). Then, we obtained

$$\left| \int_{\mu_a}^{a^*} \mathcal{N}(a|\mu_a, \sigma_a^2) f(a) da \right| = \left| \int_{a^*}^{\infty} \mathcal{N}(a|\mu_a, \sigma_a^2) f(a) da \right|. \quad (6)$$

This means that the integral of $\mathcal{N}(a|\mu_a, \sigma_a^2) f(a)$ in the range of $0 < a < a^*$ is the same as that in the range of $a > a^*$ from $g(\sigma_a^*) = 0$. In the followings, for the simple explanation, we assume $f(a) > 0$ for $0 < a < a^*$. Note that the same explanation can be provided when $f(a) < 0$ for $0 < a < a^*$. If $g(\sigma_a)$ is always 0 regardless σ_a , differential of $g(\sigma_a)$ must be 0. Then, we differentiates $g(\sigma_a)$ by σ_a , given by

$$\begin{aligned} \frac{dg(\sigma_a)}{d\sigma_a} &= \frac{d}{d\sigma_a} \int_{\mu_a}^{\infty} \mathcal{N}(a|\mu_a, \sigma_a^2) f(a) da = \int_{\mu_a}^{\infty} \frac{d}{d\sigma_a} \mathcal{N}(a|\mu_a, \sigma_a^2) f(a) da \\ &= \int_{\mu_a}^{\infty} \frac{(a - \mu_a)^2 - \sigma_a^2}{\sigma_a^3} \mathcal{N}(a|\mu_a, \sigma_a^2) f(a) da \end{aligned} \quad (7)$$

$\mathcal{N}(a|\mu_a, \sigma_a^2) f(a)$ for $a < \mu_a + \sigma_a$ becomes far from 0 with the increase in σ_a , and that for $a > \mu_a + \sigma_a$ becomes close to 0 (Supplementary Fig. 9, middle panel). Then, when σ_a slightly decreases from $\sigma_a = a^* - \mu_a$, $\int_{\mu_a}^{a^*} \mathcal{N}(a|\mu_a, \sigma_a^2) f(a) da$ becomes larger and $\int_{a^*}^{\infty} \mathcal{N}(a|\mu_a, \sigma_a^2) f(a) da$ becomes smaller. Hence, the l.h.s. of the equation (6) becomes larger and the r.h.s. of the equation (6) becomes smaller, then, $g(\sigma_a)$ increases. When σ_a decreases more, $\int_{\mu_a}^{a^*} \mathcal{N}(a|\mu_a, \sigma_a^2) f(a) da$ keeps positive value, and $\int_{a^*}^{\infty} \mathcal{N}(a|\mu_a, \sigma_a^2) f(a) da$ decreases and becomes close to 0, then, the summation of $\int_{\mu_a}^{a^*} \mathcal{N}(a|\mu_a, \sigma_a^2) f(a) da$ and $\int_{a^*}^{\infty} \mathcal{N}(a|\mu_a, \sigma_a^2) f(a) da$, i.e. $g(a)$ becomes positive value (Supplementary Fig. 9, lower panel). This means there does not exist σ_a satisfying $g(\sigma_a) \equiv 0$ for $0 < \sigma_a < a^* - \mu_a$. This is to be conflict with the assumption that there exists σ_a satisfying $g(\sigma_a) = 0$ for $0 \leq \sigma_a \leq \sigma_a^*$. Then, there does not exist σ_a satisfying $g(\sigma_a) = 0$ for $0 \leq \sigma_a \leq \sigma_a^*$. Therefore, if the equation (1) is satisfied, the equation (2) becomes not to be satisfied when CV_a slightly becomes large. Thus, under the conditions where the equation (5) in the main text is satisfied, there does not exist the distribution of Ca_{res} with the fluctuation of Amp_{PF} , $p_{ac}(Ca_{res}|\mu_a, \sigma_a)$, which does not change against the fluctuation of Amp_{PF} , indicating that the distribution of Ca_{res} changes with the increase in CV_a .



Supplementary Figure S9 | The schematic image of σ_a -dependency of $f(a)$ (upper panel), $\mathcal{N}(a|\mu_a, \sigma_a)$ (middle panel) and $\mathcal{N}(a|\mu_a, \sigma_a)f(a)$ (lower panel). When σ_a decreases from $\sigma_a = a^*$, $\mathcal{N}(a|\mu_a, \sigma_a)$ increases for $0 < a < a^*$ and decreases for $a > a^*$. Therefore, the integral of $\mathcal{N}(a|\mu_a, \sigma_a)f(a)$ for $0 < a < a^*$ increases and that for $a > a^*$ becomes close to 0.